ARTICLE | Article in Press

# Spatiotemporal analysis of shoreline changes in Mobile Bay, U.S.A.

**Fatema Tuz Johra Nourin · Hemal Dey · Wanyun Shao · Dinuke Munasinghe**

Received: 29 July 2026 / Accepted: 10 November 2026
© The Author(s) 2026

**Abstract**

Shoreline changes affect coastal communities by altering ecosystems and storm buffers. With the growth of coastal populations, the societal impact of shoreline change is expected to increase. Understanding the past and present shoreline positions is thus essential for managing coastal hazards and supporting population as well as ecosystem services. This study quantifies shoreline change rates and evaluates the persistence and variability of shoreline behavior in Mobile Bay, U.S., over the past 25 years (2000–2024 inclusive). CoastSat, an open-source Python software toolkit built on the cloud computing platform Google Earth Engine (GEE), is used to detect shoreline positions and analyze change rates. Furthermore, the Hurst exponent analysis is applied to the shoreline change rate of 396 shore-normal transects to assess the persistence or randomness of shoreline change behavior. The findings reveal substantial spatial heterogeneity in shoreline dynamics across Mobile Bay, with Dauphin Island exhibiting the highest erosion rate (−5.4 m/yr), the greatest shoreline variability between the northern and southern shore, and the strongest responses to major hurricane events. In contrast, the more sheltered estuarine shorelines towards the riverine delta experienced smaller shoreline displacements and more localized variability. The integration of persistence analysis with conventional erosion-accretion assessments enabled the distinction between persistently erosional, persistently accretional, and highly variable shoreline segments, providing additional insight into long-term and short-term shoreline behavior. The findings contribute to a more comprehensive understanding of shoreline dynamics and support site-specific coastal management, hazard mitigation, and the implementation of nature-based solutions.

**Keywords** CoastSat · Coastal management · Google Earth engine · Hurst exponent · Remote sensing · Tidal correction

## Introduction

The coastal environment is dynamic in nature, driven by natural processes and human activities. Shorelines play a vital role in the coastal environment and communities worldwide, providing buffers against natural hazards and critical habitats for many species of flora and fauna[1]. Shoreline positions around the world are experiencing significant changes, driven by both natural and anthropogenic factors, including coastal morphology and sediment

This Article in Press is shared early to give you faster access to new research. It is citable and carries a permanent DOI. The final edited version will replace it automatically.



https://doi.org/10.1038/s41598-026-80664-1

Published online: 15 November 2026

scientific reports

availability, sea level rise, geotectonic movements, wind, ocean waves, natural disasters, and tidal changes, as well as man-made infrastructure such as shoreline stabilization, coastal development, and dredging[2–4]. From 1984 to 2016, a global analysis found that 24% of the world's sandy shorelines persistently eroded at rates exceeding 0.5 m/yr. Even within marine protected areas, 37% of the sandy shorelines eroded[5]. Similarly, a 32 -year global shoreline study (1984–2015) found erosion of 28,000 square km, which was almost twice the area of accretion, and found anthropogenic activities and natural hazards to be the major drivers of shoreline change[6]. As coastal populations increase, the impact of shoreline erosion on coastal communities is expected to grow[7,8]. Therefore, a comprehensive assessment of the spatial and temporal variability of shoreline changes at the local scale is as crucial as at the global scale for effective coastal management[1], as its locally tailored assessment can provide critical insights.

Various tools and techniques have been employed in recent years to monitor coastal erosion and coastline changes. Many of these tools are geographic information systems (GIS) based, utilizing both proprietary software, e.g., ESRI ArcGIS, and the Digital Shoreline Analysis System[9], as well as open-source platforms, e.g., QGIS and the Open Digital Shoreline Analysis System Against this backdrop, shoreline change detection research has shifted towards spatiotemporal analysis of high-resolution satellite imagery, driven by the availability of multispectral imagery at different temporal frequencies[10,11]. Beyond remote sensing, the rise of artificial intelligence has opened a new frontier, enabling automated large-scale shoreline extraction[12]. These advanced techniques enhance the analysis of complex environmental datasets, identify patterns and trends that are challenging to detect with traditional methods, and support the development of predictive models to forecast coastal ecosystem responses to environmental pressures[13]. By leveraging these advanced tools, it is possible to address key challenges such as detecting subtle changes, predicting future coastal dynamics, and improving resilience against coastal hazards[14]. Some of the contemporary shoreline change studies have applied these advanced tools across a wide range of coastal settings to quantify erosion and accretion rates. Multi-decadal satellite analyses of global shoreline monitoring found more erosion than accretion, with pronounced spatial variability driven by human activities and natural hazards[5,6], while regional monitoring found storms, sea-level rise, sediment supply, and human interventions[7,15] as the drivers of change.

The recent development of the CoastSat, an open-source Python toolkit, has enabled automated shoreline extraction from Landsat and Sentinel imagery over large spatial and temporal scales[16]. The CoastSat toolkit has been applied in diverse coastal environments worldwide, including long-term shoreline erosion and accretion trends, shoreline response to storms, and coastal vulnerability assessments[11,16]. For example, Souiri et al.[17] analyzed 30 years of satellite imagery using the CoastSat toolkit and revealed significant erosion along Morocco's entire coastline, with the most severe rates (greater than −2 m/yr) around the mouth of Oued Laou. Using the same toolkit,[18] detected heterogeneous shoreline change patterns along the Río de la Plata estuary in Argentina from 1984 to 2023, showing a shift from erosion (1984–2003) to slight accretion (2003–2023). Moreover, Gunasinghe et al.[19] applied the CoastSat toolkit along the west coast of Sri Lanka and found that the area north of Mount Lavinia Beach accreted by 18–27 m, while the area south of the beach experienced erosion of 12–17 m between 2015 and 2021. Another study by Curoy et al.[20] spanning over 29 years in Thailand found a significant connection between extreme weather and shoreline erosion, while a recent study by Asare-Bediako et al.[21] in the eastern coast of Ghana revealed substantial regional variation in shoreline dynamics.

Along the U.S. Gulf Coast, population growth and urban expansion have accelerated land use landcover (LULC) changes, placing increasing pressure on coastal wetlands and contributing to habitat loss and alterations in land and water systems[1,22]. Degradation of ecosystem services in the Mobile Bay area in particular poses a significant threat to the national economy, as the region is crucial for energy production, navigation, and commercial and recreational activities[23]. Mobile Bay is a major economic hub supporting one of the nation's largest inland port systems, but it is highly vulnerable to hurricanes, storm surges, flooding, and sea-level rise[24]. Major hurricane events along the[25], Georges (1998),[26–28]- have significantly affected Mobile Bay[25,29]. Mobile Bay's geomorphic and hydrological complexity produces strong spatial variation in shoreline behavior, driven by Gulf

wave exposure, riverine sediment deposition, and compound flooding from storm surge, rainfall, and river discharge[30–32]. These natural processes interact with human intervention, which includes navigation, dredging, and infrastructure development, which can alter local sediment transport and shoreline response[33]. This dynamic setting renders Mobile Bay an ideal test bed for assessing spatiotemporal shoreline change and informing adaptive coastal management strategies, including Nature-Based Solutions (NBS).

Efficient coastal management requires comprehensive data to capture the dynamic nature of the coastal environment. Currently, NOAA's National Shoreline and Continually Updated Shoreline Product (CUSP) provides authoritative representations of the U.S. shoreline and is widely used for navigation, coastal planning, hazard assessment, and environmental monitoring[34]. However, NOAA shoreline products are designed primarily as baseline current-shoreline datasets rather than as continuous shoreline-change monitoring systems. The dataset is updated as new source data become available, but it does not explicitly quantify shoreline migration rates, erosion–accretion dynamics, or the drivers of shoreline change through time.

Despite advances in shoreline monitoring using remote sensing, GIS, and machine learning techniques and existing products, there remains a gap in capturing shoreline evolution across different temporal scales and in accounting for differences in variability and change dynamics, especially in densely populated, ecologically significant coastal areas such as Mobile Bay. For effective coastal management that caters to dynamic diversity, it is important to examine the differences and similarities in the persistence of shoreline change across diverse geomorphological coastal environments. Persistence of shoreline change is the tendency for shoreline change to occur in the same direction, as opposed to random or event-driven shoreline change behavior. To address this critical research gap, this study seeks to answer the question: How has shoreline change varied spatially and temporally across Mobile Bay over the past 25 years? In hazard research, multi-decadal records of approximately 25–30 years are generally recognized as suitable for long-term assessments because they capture trends while reducing the influence of short-term variability and episodic events[35,36].

Specifically, this study aims to: (i) quantify shoreline erosion and accretion patterns using satellite-derived shoreline positions, (ii) evaluate the persistence and variability of shoreline change behavior through Hurst exponent analysis. The aforementioned CoastSat toolkit, endpoint analysis, and persistence analysis are used in this study along shore-normal transects to examine shoreline dynamics in Mobile Bay.

The novelty of this study lies in integrating shoreline persistence analysis with typical change-rate analysis, enabling the capture of episodic and persistent erosion-accretion change rates. The shore-normal transects allow for the assessment of spatial and temporal heterogeneity. While the existing shoreline products available for Mobile Bay provide valuable shoreline position, they do not provide the trend and direction of shoreline movement. By integrating dense transect-based analysis, this study distinguishes between persistent erosion, persistent accretion, and comparatively stable and highly variable shoreline segments. Therefore, this study provides a more comprehensive understanding of shoreline dynamics for Mobile Bay, which is valuable for identifying vulnerable or comparatively stable shoreline segments. These findings provide valuable information for organizations involved in coastal management and restoration in Mobile Bay to support shoreline monitoring, habitat restoration, and dredging, and site-specific NBS shoreline rehabilitation measures. The approach can be transferred to other dynamic coastal systems[37].

## Methodology

### Study area

Mobile Bay, located on Alabama's northern Gulf Coast, is one of the largest estuaries in the United States. Formed by the confluence of the Mobile, Tensaw, Alabama, and Tombigbee Rivers, the Bay drains into the Gulf of America through a narrow inlet between Dauphin Island and the Fort Morgan Peninsula[38]. The Bay region comprises Mobile and Baldwin Counties, with representative geographic coordinates of approximately 30.68° N, 88.20° W

and 30.66° N, 87.75° W, respectively, and a population of 414,809 and 231,767, respectively (U.S.[39]). Mobile Bay is an ecologically, hydrologically, and economically significant region[40]. The surrounding coastal landscape includes wetlands and estuarine habitats along with developed and industrial areas, with major economic activities of commercial shipping, fisheries, tourism, and recreation[41]. Its watershed ranks fourth in freshwater discharge among the continental U.S. watersheds, strongly influencing estuarine processes[42,43]. Morphometrically, Mobile Bay has an area of approximately 1070 square km, with a length of approximately 50 km, and a width of[44] approximately 39 km. The study area is a relatively shallow Bay area with a mean depth of approximately 3 m and a microtidal[45] range of 0 to 0.6 m.

Mobile Bay is surrounded by a highly developed and densely populated region, yet it encompasses diverse coastal environments, including barrier islands, tidal marshes, estuaries, dunes, wetlands, and urban shorelines. In addition, this region has high exposure to hurricanes, compound flooding, and storm surge[24], making the coastline highly vulnerable to coastal hazards. These coastal hazards, coupled with sea level rise, can cause rapid shoreline retreat, dune breaching, and sediment redistribution[46,47].

Meanwhile, Dauphin Island acts as a natural barrier that protects Mobile Bay from strong Gulf wave energy, yet it is itself highly susceptible to shoreline erosion[29,48]. Along the open ocean shoreline, there were erosion rates ranging from about 1.5 to 4 m/yr in the past 75-year period from 1940 to 2015[49]. In contrast, the more sheltered eastern shoreline near Daphne and Fairhope experiences lower wave energy, where estuarine sediment deposition often promotes localized shoreline accretion[42,43]. For example, near Daphne, the shoreline between Village Point and Ragged Point accreted at 0.09 m/yr between 1981 and 2011[50]. These dynamic coastal processes and spatially heterogeneous shoreline changes make the Mobile Bay region an ideal setting for investigating shoreline changes. Figure 1 shows the geographic context and extent of the study area.

## Data source

This study utilized secondary data for analyzing the shoreline positions in Mobile Bay. The list of data sources is shown in Table 1.

## Methods

To ensure consistent shoreline extraction and robust long-term trend characterization, this study consists of three major stages: (i) delineation of shoreline positions, (ii) tidal correction and adjustment of shoreline positions, and (iii) analysis of shoreline change type. Each stage integrates multiple data sources and analytical steps, which are described briefly below.

### Delineation of shoreline positions

Shoreline positions for Mobile Bay were extracted using the CoastSat toolkit developed by Vos et al.[16]. The analysis was conducted using the CoastSat Python toolkit, which uses the Google Earth Engine (GEE) API to retrieve and process satellite imagery. Mobile Bay was first defined as the region of interest (ROI), the temporal range was set from January 2000 to December 2024, and Landsat Collection 2 Tier 1 surface reflectance products from Landsat 5, 8, and 9 were selected to provide consistent, radiometrically calibrated, and geometrically accurate images for shoreline extraction. Within the CoastSat Python toolkit, image preprocessing involved retrieving satellite imagery from the GEE API, spatial clipping to the defined Mobile Bay extent, and applying cloud masking with a threshold of 10% or less to maximize image clarity. Pan-sharpening was applied to improve spatial detail and enhance shoreline accuracy. To minimize the processing time, the study area was subdivided into six ROIs based on their morphological differences (Fig. 7), and the same workflow was applied in all six ROIs. In the processed satellite imagery, the Modified Normalized Difference Water Index (MNDWI)[51] was used to extract shoreline positions. Here, shoreline positions were extracted from all available Landsat Surface Reflectance

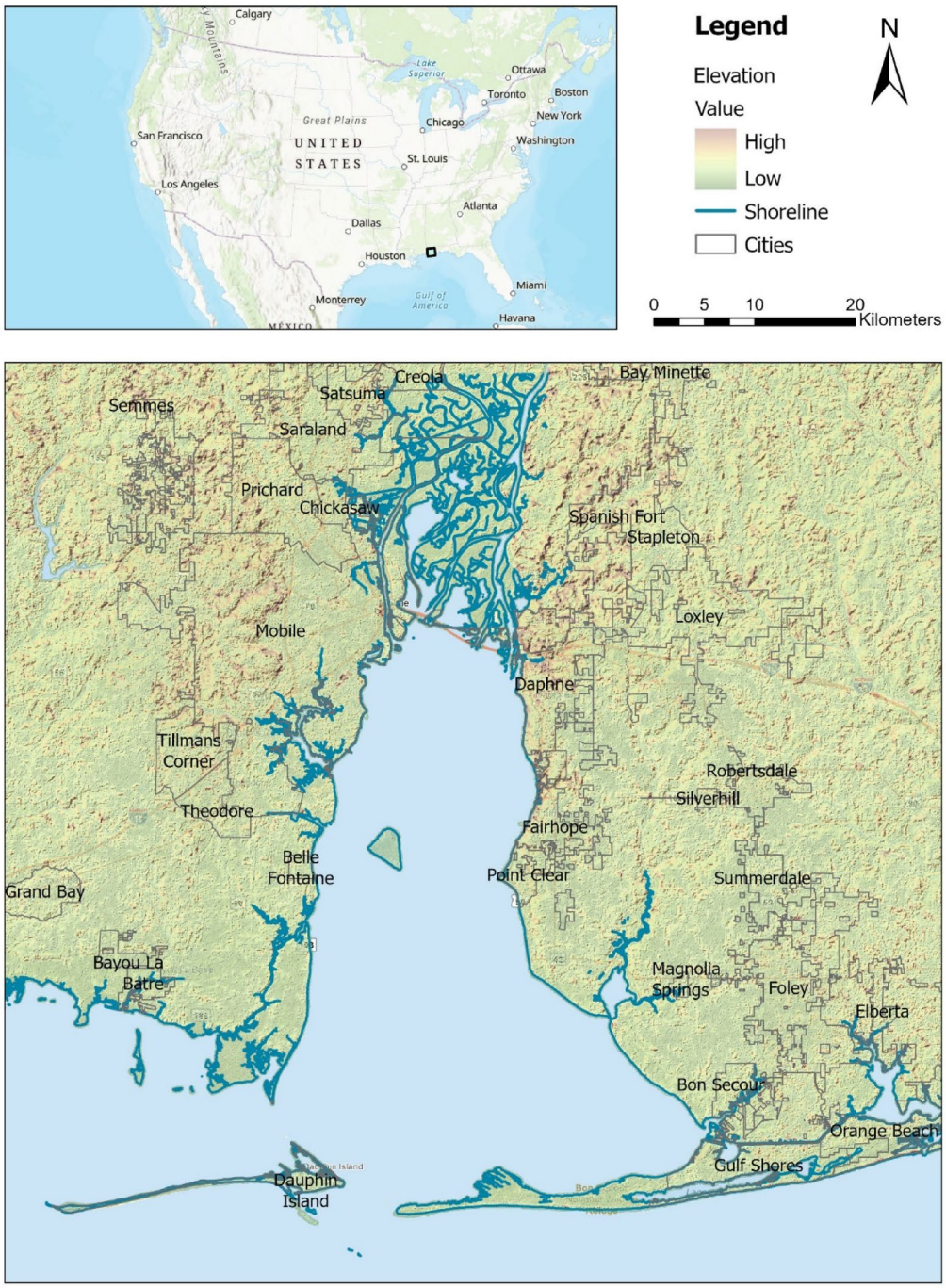



**Fig. 1** Map of the study area map generated using ArcGIS Pro (version 3.7.0; Esri, https://www.esri.com/en-us/arcgis/products/arcgis-pro/overview.

images acquired between January 2000 and December 2024, with cloud cover at or below 10%. Thus, the temporal spacing between successive shoreline observations varied with the Landsat revisit schedule and image availability. Consequently, Monthly shoreline positions were generated when one or more suitable images were available within a given month.

The MNDWI indices enhanced the contrast between water and non-water surfaces. The MNDWI is calculated as follows:

**Table 1** Description of the data used in the study.

| Data component | Data type | Data format | Data source | Analysis method |
|---|---|---|---|---|
| Satellite Image selection | Landsat 4–5 TM, Landsat 8 OLI, Landsat 9 OLI-2 | Raster | Secondary: Google Earth Engine archive | Computation of the Modified Normalized Difference Water Index (MNDWI) and multi-temporal shoreline extraction over a 25-year period |
| Reference Shoreline | User-defined points to capture shoreline curvature | Vector | Primary: Manual digitization using the CoastSat graphical user interface (GUI) | Shoreline extraction of 25 years |
| NOAA Tide Level Data | Tidal and water level time-series data | Tabular (JSON / CSV via API) | Secondary: NOAA Tides and Currents API | Time-series analysis and Hurst exponent–based long-term persistence analysis |
| Beach Slope | Digital Elevation Model (DEM) | Raster | Secondary: SRTM 1 Arc-Second Elevation Model | Tidal correction using estimated beach slope and a reference elevation to normalize cross-shore shoreline position time series |

$$MNDWI = (SWIR1 - G)/(SWIR1 + G) \quad (1)$$

Here, SWIR1 represents the pixel intensity of the short-wave infrared band, and G represents the pixel intensity of the green band. Also, the MNDWI values range from -1 to 1, where -1 indicates water and positive values indicate non-water surfaces[16].

Following the CoastSat workflow[16], a pretrained Multilayer Perceptron (MLP) classifier was applied to each retrieved satellite image to create a land-cover mask with four classes: sand, water, white water, and other land features. The classifier, developed and validated by Vos et al.[16], was combined with the Modified Normalized Difference Water Index (MNDWI) to improve the identification of the land–water interface. The MNDWI thresholding provided an initial binary land–water separation, while the MLP classification reduced any misclassification caused by water, white water, wet sand, and other features with similar spectral values using the land cover mask. Shoreline positions were then extracted from the resulting land–water interface for each acquisition date, producing a dense multi-temporal dataset of shoreline vectors. According to Vos et al.[16], the CoastSat workflow, the combination of the MNDWI and the pretrained MLP classifier, can delineate the land–water interface with sub-pixel shoreline mapping capability, which was built upon the sub-pixel border segmentation by Liu et al.[52].

To validate the positional agreement of the extracted shorelines, an image-based comparison was conducted for a subset of Dauphin Island using manually digitized reference shorelines from higher-resolution aerial imagery from Google Earth. The reference shorelines were digitized within Google Earth by visually tracing the land–water boundary on the selected historical images. The resulting shoreline features were exported as KMZ files, imported into ArcGIS Pro, and converted to GIS-compatible vector features for comparison with the Landsat-based CoastSat-derived shorelines. Two validation periods, representing an earlier (2000) and a more recent period (2020) of the study, were selected. For the 2000 comparison, the reference shoreline was digitized from Google Earth imagery acquired on March 21, 2000, and compared with the CoastSat-derived shoreline from Landsat imagery acquired on March 10, 2000, resulting in an 11-day temporal offset. For the 2020 comparison, the reference shoreline was digitized from Google Earth imagery acquired on December 31, 2020, and compared with the CoastSat-derived shoreline from Landsat imagery acquired on December 17, 2020, resulting in a 14-day temporal offset. Then, the shorelines derived both from the aerial image and CoastSat were intersected with the same shore-normal transects, and 40 transects intersecting both shorelines were retained for each validation period. The planar distance between corresponding reference and CoastSat intersection points was calculated for each transect. Positional agreement was quantified using mean absolute error (MAE) and root mean square error (RMSE).

$$MAE = \frac{1}{n}\sum_{i=1}^{n}|e_i|$$

$$RMSE = \sqrt{\frac{1}{n}\sum_{i=1}^{n}e_i^2}$$

where $e_i$ represents the positional difference between the reference and CoastSat-derived shoreline at transect i, and n represents the number of matched transects (40).

Later, shoreline change was quantified by intersecting the extracted shoreline positions with 396 shore-normal transects along approximately 800 km of analyzed shoreline across the six ROIs. The shoreline length was analyzed in ArcGIS Pro by projecting the shoreline shapefile to NAD 1983 UTM zone 16N and then summing the lengths of the shoreline features. The shore-normal transects were manually digitized in the CoastSat GUI to provide comprehensive spatial coverage of each ROI. From a clear reference image, transects were drawn perpendicular to the shoreline from landward to seaward and distributed along the entire shoreline segment to capture local variability. The transect spacing was not fixed; the number and spacing of transects in each ROI varied according to the geometry and the length of each ROI. Cross-shore shoreline shift measurements were taken along each transect. The workflow is shown in Fig. 2, and the different stages of shoreline delineation are shown in Fig. 3:

### Tidal correction and quantification of shoreline erosion and accretion patterns

The shorelines extracted over 25 years in the previous stage were influenced by tidal effects at the time of satellite image acquisition. To account for this effect, shoreline positions were tidally corrected using NOAA tidal predictions. Hourly tidal predictions referenced to Mean Sea Level (MSL) were obtained from NOAA CO-OPS stations 8,729,840, 8,735,180, 8,736,897, and 8,737,048 for the 2000—2024 study period. Station 8,729,840 was used for ROIs a and f; station 8,735,180 for ROI b; station 8,736,897 for ROI c; and station 8,737,048 for ROIs d and e. For each image acquisition date, the corresponding predicted tidal level was obtained from the NOAA tidal time series and used for tidal correction. Shoreline positions were then corrected to the common reference elevation of Mean Sea Level (MSL) using the corresponding tidal level and the site-specific beach slope. ROI specific beach slope values were derived from an SRTM 1 Arc-Second Global Digital Elevation Model (spatial resolution of 30 m) obtained from the U.S. National Map in 2000. Mean slope values for the ROIs were estimated using the zonal statistics tool in ArcGIS Pro and used as a static input to the CoastSat tidal correction workflow throughout the 2000 to 2024 study period. The mean DEM-derived beach slopes for ROIs a to f were 0.04, 0.02, 0.04, 0.04, 0.05, and 0.04, respectively. This study did not incorporate temporal changes in beach slope into the tidal correction.

The vertical tidal difference between the observed water level at the time of image acquisition and the datum was converted to a horizontal correction using the representative slope, and the corrected value was added to the cross-shore shoreline positions measured along each shore-normal transect. This tidal correction normalized the shoreline position time series to a common reference elevation (datum), allowing for more accurate assessment of shoreline movements over time. A conceptual tidal correction and a representative transect showing the raw observed values and corrected values are shown in Fig. 4.

After delineation of the shoreline positions, the Net Shoreline Movement (NSM) and the End Point rate (EPR;[9]) commonly used in the Digital Shoreline Analysis System (DSAS) were analyzed as follows:

$$NSM = Distance_{latestshoreline} - Distance_{earliestshoreline} \quad (2)$$

$$EPR = \frac{NSM}{yearsbetweenoldestandnewestshoreline} \quad (3)$$

https://doi.org/10.1038/s41598-026-80664-1

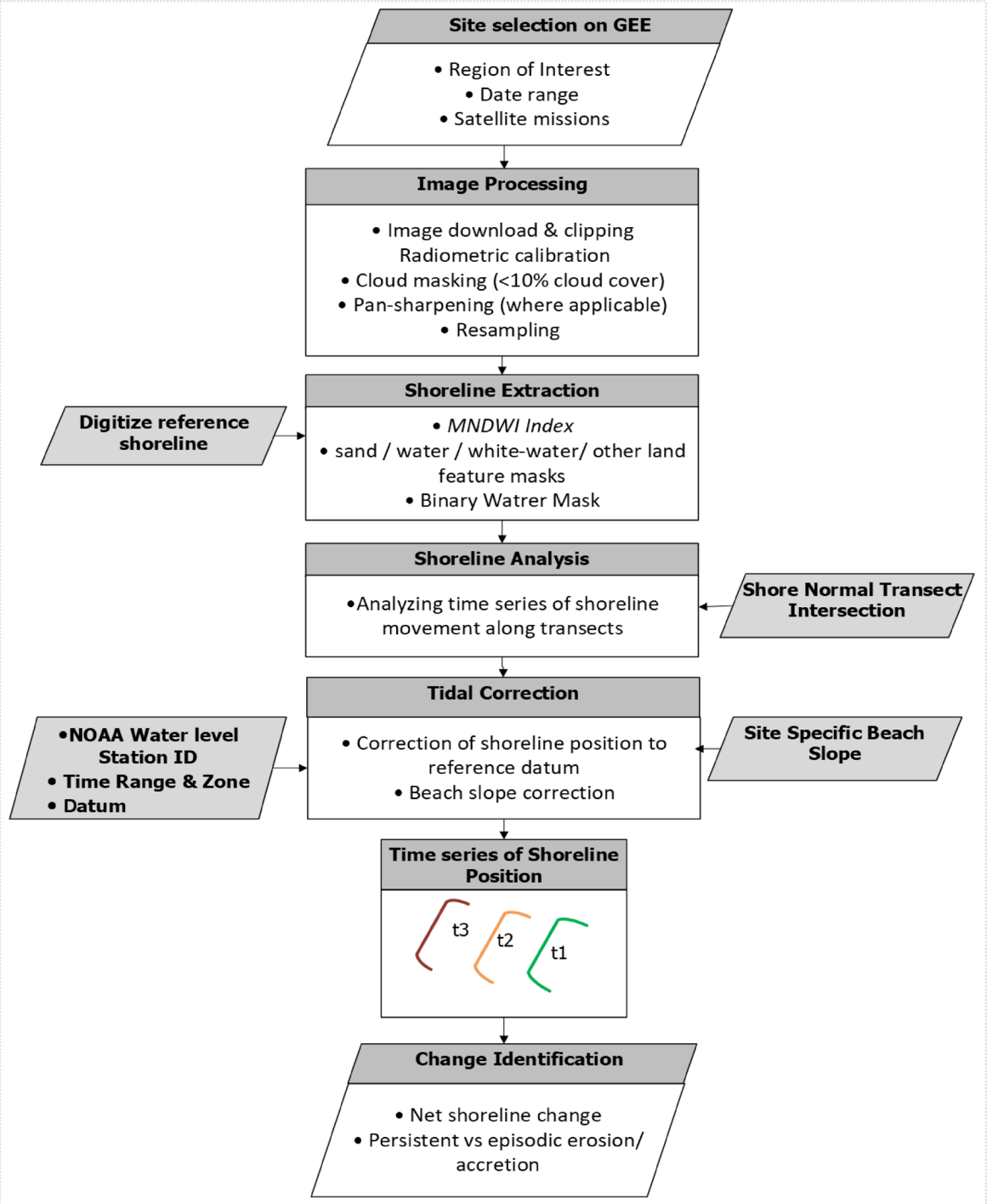



**Fig. 2** Methodological framework for shoreline change analysis.

### Evaluation of the persistence and variability of shoreline behavior

Following tidal correction, shoreline positions extracted along each shore-normal transect were assembled for time series analysis corresponding to successive image acquisition times ($t_1$, $t_2$, …, $t_n$). These time series were then analyzed to characterize the direction and persistence of shoreline change. Hurst Exponent (H) is a statistical measure used to assess the long-term memory or persistence of a time series. Along each shore-normal transect,

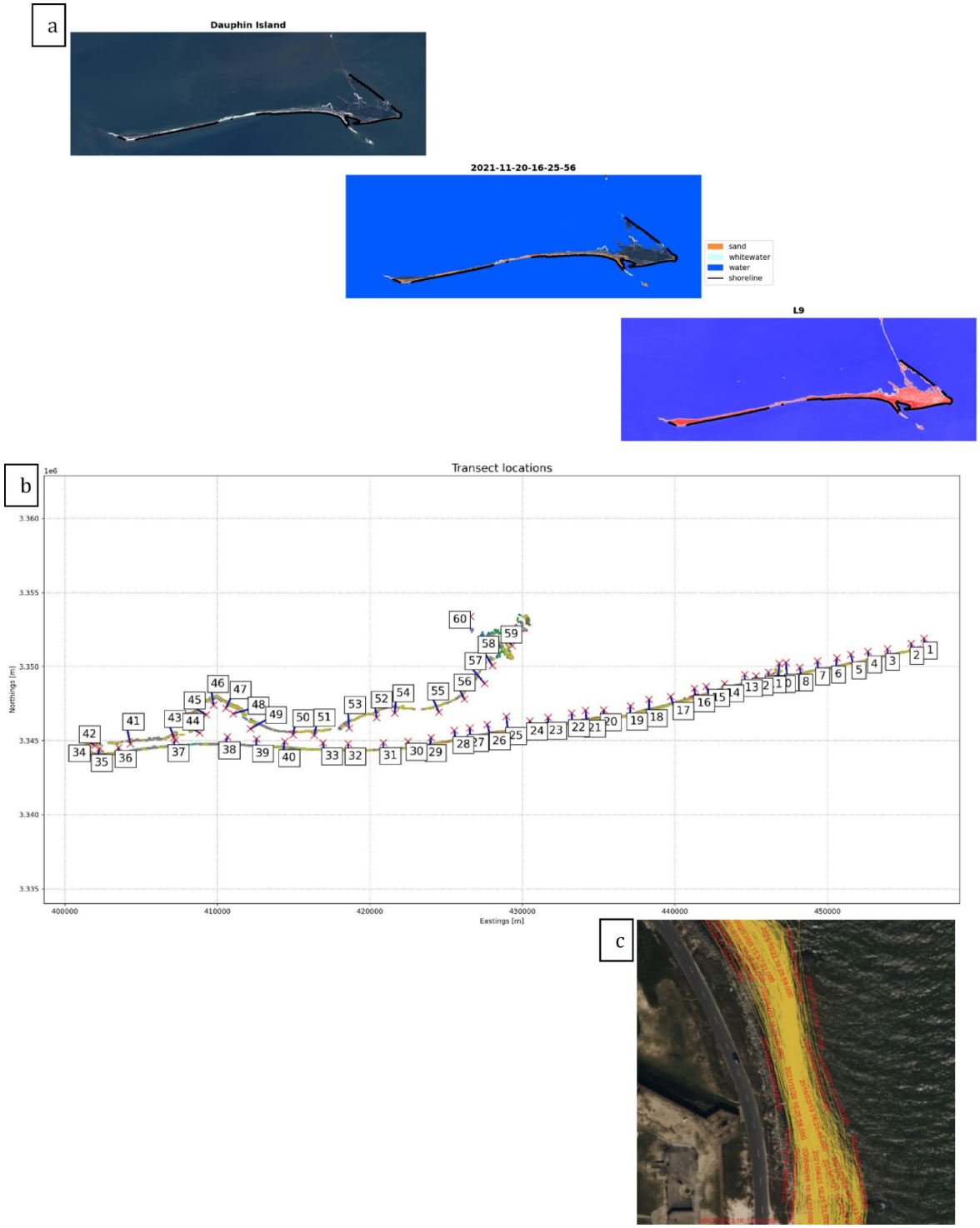



**Fig. 3** Different stages of Shoreline Delineation. (**a**) shows the delineation of the shoreline based on the digitized reference shoreline and the land cover masks. (**b**) shows the shore-normal transects drawn from landward to seaward direction on the GUI. (**c**) c shows the time-enabled shorelines derived as the output.

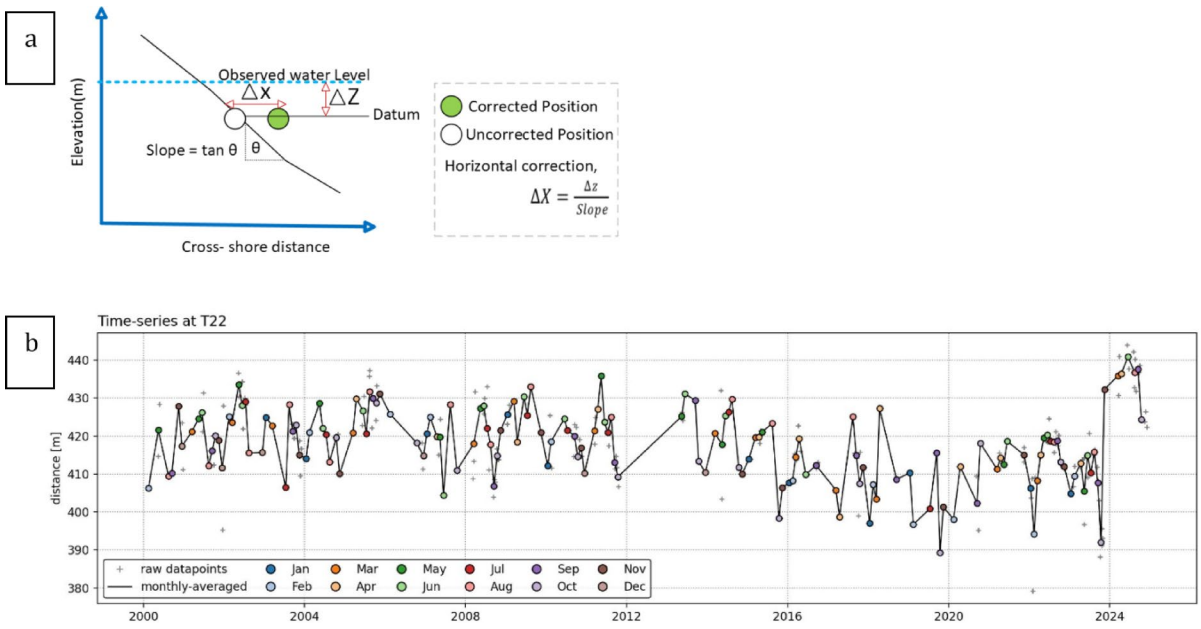



**Fig. 4** (**a**) Conceptual diagram showing the conversion of the vertical tidal difference to a horizontal shoreline correction using the representative beach slope. (**b**) Representative shoreline position time series extracted by CoastSat for a shore-normal transect, including the raw shoreline observations and the tidally corrected shoreline positions.

the Hurst Exponent was utilized to assess the long-term persistence of shoreline change behavior. Although Landsat revisit time is 16 days, the availability of suitable images was irregular due to cloud cover. So, the observations were aggregated into monthly time steps. When multiple observations occurred within a month, the mean shoreline position was used. For short temporal gaps of up to two months, observations were interpolated using linear interpolation. Remaining missing gaps were excluded from the calculation of the Hurst exponent. The Hurst Exponent is defined as-

$$E\left[\frac{R(n)}{S(n)}\right] = C\,n^{H} \tag{4}$$

Here, **R(n)** = the range of cumulative deviations of shoreline positions from the mean shoreline position over a given time period, **S(n)** = the standard deviation of shoreline positions for the same period, **E[x ]** = the expected rescaled range value of the shoreline position time series, **n** = the number of shoreline observations or time steps in the shoreline position time series, **C** = a constant, **H** = the Hurst Exponent, which describes the long-term persistence behavior of shoreline change. The Hurst exponent (H) was estimated for each transect using rescaled-range (R/S) analysis. The analysis was performed across multiple window lengths, ranging from eight time steps to approximately half of the available time-series length. For each window length, the R/S value was calculated using non-overlapping segments, with at least two segments required for inclusion. A minimum of six valid window lengths was required to estimate H. The Hurst exponent was calculated as the slope of the linear regression between log(R/S) and log(n), where n represents the window length. The **H** value is interpreted as: i) $H > 0.5$: persistent, ii) $H = 0.5$ (approximately): random, iii) $H < 0.5$: anti-persistent. Values of the Hurst exponent were used to distinguish between persistent processes, anti-persistent behavior, and random or episodic variability in shoreline dynamics. Hurst values enabled characterization of temporal persistence, while the direction of the shoreline change- erosion or accretion was determined from the shoreline change rate. Transects with a positive shoreline change rate (accretion) were assigned a directional value of + 1, whereas transects with a negative shoreline change rate (erosion) were assigned a value of -1. The directional value was multiplied by the Hurst exponent to produce a signed Hurst value, in which the sign represented the direction of shoreline change and

the magnitude retained the Hurst-based persistence information. Together, these two metrics were considered to characterize the direction and persistence of shoreline change along each transect. Additionally, shoreline change was quantified to summarize overall shoreline movement over the study period.

To assess the sensitivity of the Hurst exponent estimates to temporal interpolation, two supplementary analyses were conducted for Dauphin Island (ROI b) using observed shoreline positions. First, the annual mean shoreline positions were calculated without interpolation, and Hurst exponents were estimated from the longest consecutive sequence of observed years. Second, the Hurst exponents were calculated from the longest uninterrupted sequence of observed monthly shoreline positions. To accommodate the shorter uninterrupted time series, the minimum R/S window length was reduced from eight to three time steps, and the minimum number of window sizes required to estimate the scaling relationship was reduced from six to three. The resulting Hurst estimates and persistence classifications were compared with those obtained using the original monthly approach.

### Uncertainty and sensitivity assessment

Satellite-derived shoreline positions are subject to uncertainties associated with georeferencing, spatial resolution, image acquisition time, cloud cover, shoreline-detection procedures, etc. Previous independent validation of the CoastSat methodology against on-site shoreline measurements reported horizontal shoreline-position RMSE values of approximately 7.3–12.7 m across multiple validation sites[16], indicating the positional accuracy threshold achievable with CoastSat. This study utilized the upper value of 12.7 m as a conservative literature-based positional uncertainty benchmark for interpreting the magnitude of shoreline change. Then, the uncertainty in NSM and EPR was estimated by propagating this positional uncertainty benchmark of the two endpoint shoreline positions using the root-sum-square approach[9], resulting in an NSM uncertainty benchmark of 17.96 m.

$$Uncertainty_{NSM} = \sqrt{Uncertainty_{start}{}^2 + Uncertainty_{end}{}^2}$$

Because EPR was calculated by dividing NSM by the time between the first and last valid shoreline observations for each transect, the corresponding EPR uncertainty was calculated as-

$$Uncertainty_{EPR} = \frac{Uncertainty_{NSM}}{\Delta time}$$

Across the six ROIs, median EPR uncertainty ranged from 0.72 to 0.75 m/yr, while transect-specific values ranged from 0.72 to 1.62 m/yr. Then, the raw and tidally corrected shoreline positions were compared for all six ROIs using the acquisition dates and transects to quantify the sensitivity of shoreline positions to tidal correction. The absolute difference between the raw and corrected shoreline positions was used to characterize the magnitude of the tidal adjustment. Median absolute tidal adjustments ranged from 1.67 m to 11.17 m across the six ROIs, while the absolute maximum adjustments ranged from 5.03 m to 19 m. Among all ROIs, ROI d exhibited the largest sensitivity, with a median absolute adjustment of 6.85 m and an absolute maximum adjustment of 19 m.

For persistence analysis, the goodness of fit of the log–log regressions used to estimate the Hurst exponent was evaluated using the coefficient of determination ($R^2$). Across the six ROIs, median $R^2$ values ranged from 0.96 to 0.98, indicating generally strong linear fits to the R/S scaling relationships for transects with valid Hurst estimates. The ROI-specific 5th-percentile $R^2$ values ranged from 0.86 to 0.95, while the minimum individual $R^2$ was 0.83. These goodness-of-fit statistics evaluate the linear scaling relationship used to estimate Hurst values but do not account for uncertainty associated with irregular temporal sampling and short-gap interpolation.

Lastly, the hurricane-related shoreline displacement was calculated as the difference between two shoreline positions. So, the same 17.96 m propagated positional uncertainty benchmark was applied to the pre- and post-hurricane displacement estimates.

## Results

This section presents the results of the shoreline change analysis, organized into subsections that include quantification of shoreline erosion and accretion patterns from satellite-derived shoreline positions, evaluation of the persistence or randomness of shoreline change behavior, and analysis of shoreline position across different temporal scales.

### Quantification of shoreline erosion and accretion patterns

After delineating the shoreline positions of 25 years and applying the tidal corrections, the mean shoreline change rate per year was mapped using the Net Shoreline Movement (NSM) and End Point Rate (EPR) matrices and shown in the Fig. 5. The positional comparison between the CoastSat-derived and aerial image-derived reference shorelines included 40 matched transects for each validation period within a subset of the Dauphin Island shoreline. For 2000, the MAE and RMSE were 35.44 m and 40.51 m, respectively; for 2020, they were 22.99 m and 28.28 m. The median positional differences were 34.04 m in 2000 and 20.21 m in 2020.

Figure 5 shows that most shoreline segments in Mobile Bay exhibit low to moderate rates of change ranging from erosion of -0.01 to -0.85 m/yr or accretion of 0.1 to 0.86 m/yr. The inward, riverine, and estuarine-dominated parts of the bay exhibit lower shoreline change rates. In contrast, Dauphin Island exhibits the highest spatial variability in shoreline change, with alternating zones of erosion and accretion and a maximum erosion of -5.4 m/yr. Similarly, the Bon Secour Bay inlet area shows a higher accretion rate compared to the surrounding shoreline sections. Localized accretion is observed along portions of the eastern shoreline near Daphne and Fairhope.

A clear difference is observed between the northern and southern shorelines of Dauphin Island (Fig. 6). The northern shoreline, protected by the estuarine environment, has a lower per-year shoreline change rate, suggesting comparatively stable conditions. The mean shoreline change rate per year is 0.27 m/yr, with a standard deviation of 1.22 m/yr. The southern shoreline, directly exposed to Gulf wave energy and storm activity, experiences substantially higher erosion rates and greater shoreline variability. The mean shoreline change rate per year is -0.50 m/yr, with a standard deviation of 2.34 m/yr.

To examine shoreline change trends, the study area was divided into six smaller Regions of Interest (ROIs) according to differences in geomorphology from Bon Secour Bay clockwise, labeled “a” to “f,” as shown in the Fig. 7. The table presents descriptive statistics to provide an overview of erosion/accretion patterns and ranges across these six ROIs.

The summary statistics shown in Table 2 further show the spatial variability among the six selected ROIs. Dauphin Island ROI b has the highest shoreline variability and the strongest erosional behavior, with a mean shoreline change rate of −0.40 m/yr and the largest standard deviation (2.48 m/yr). In contrast, ROI a, located near the Bon Secour Bay inlet, shows an overall accretional pattern with a positive mean shoreline change rate of 0.33 m/yr. The standard deviation is also high compared to the other sites (1.83 m/yr). The other four ROIs- c, d, e, and f are within the estuarine shorelines at the northern and central portions of Mobile Bay and have a lower magnitude of shoreline change compared to the Gulf-facing coastal systems. Among these four ROIs, ROI d shows the highest positive mean shoreline change rate of 0.75 m/yr. ROIs e and f both have relatively low standard deviation values, suggesting comparatively stable shoreline conditions despite a few localized erosion or accretion patterns. ROI c exhibits near-stable shoreline behavior with a slightly negative mean shoreline change rate of -0.05 m/yr. Overall, breaking the study area down into smaller ROIs helps to understand the spatially heterogeneous shoreline dynamics in Mobile Bay.

### Evaluation of the persistence and variability of shoreline behavior

The map in Fig. 8 shows the spatial distribution of shoreline-change persistence across Mobile Bay. Persistent erosion is concentrated along Dauphin Island, while several northern and central estuarine shoreline segments

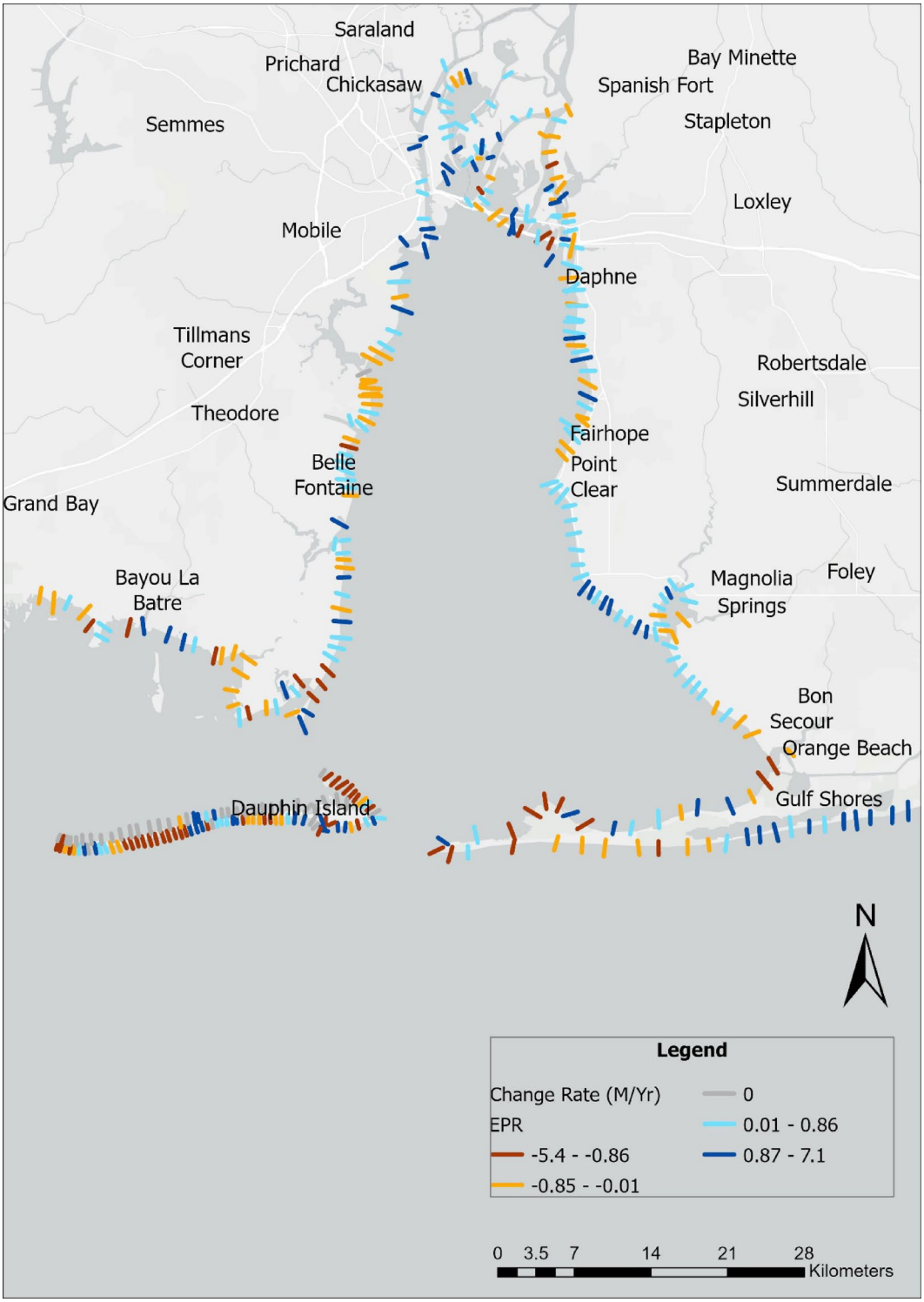



**Fig. 5** Map of Mean Yearly Shoreline Change Rate Along the Shore-Normal Transects. Map generated using ArcGIS Pro (version 3.7.0; Esri, https://www.esri.com/en-us/arcgis/products/arcgis-pro/overview.

https://doi.org/10.1038/s41598-026-80664-1

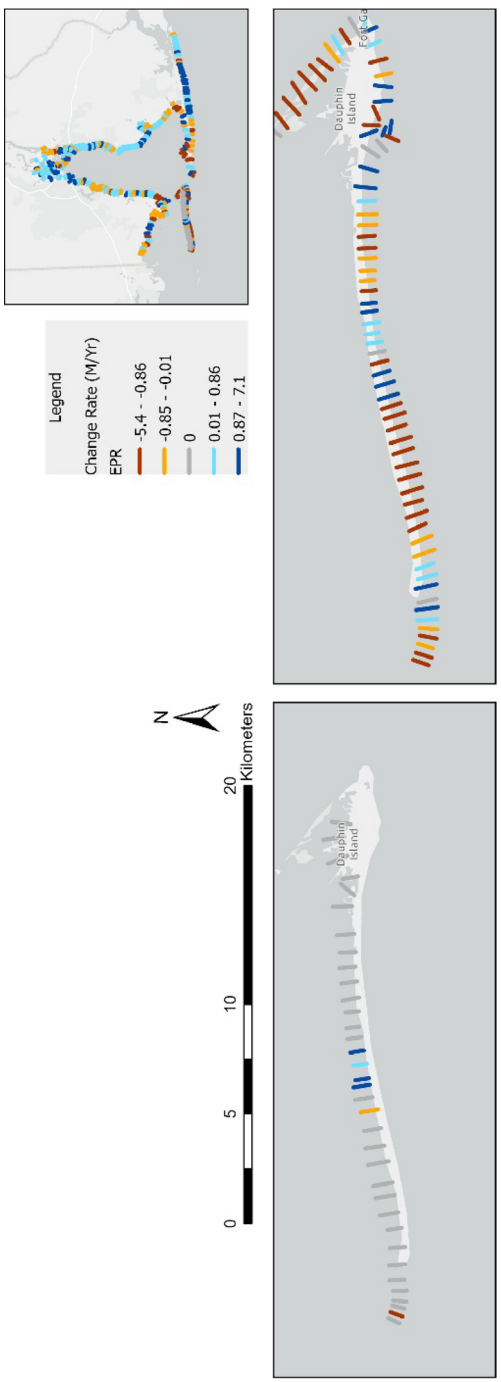



**Fig. 6** Heterogeneity in the Northern and Southern Shores of Dauphin Island. Map generated using ArcGIS Pro (version 3.7.0; Esri, https://www.esri.com/en-us/arcgis/products/arcgis-pro/overview.

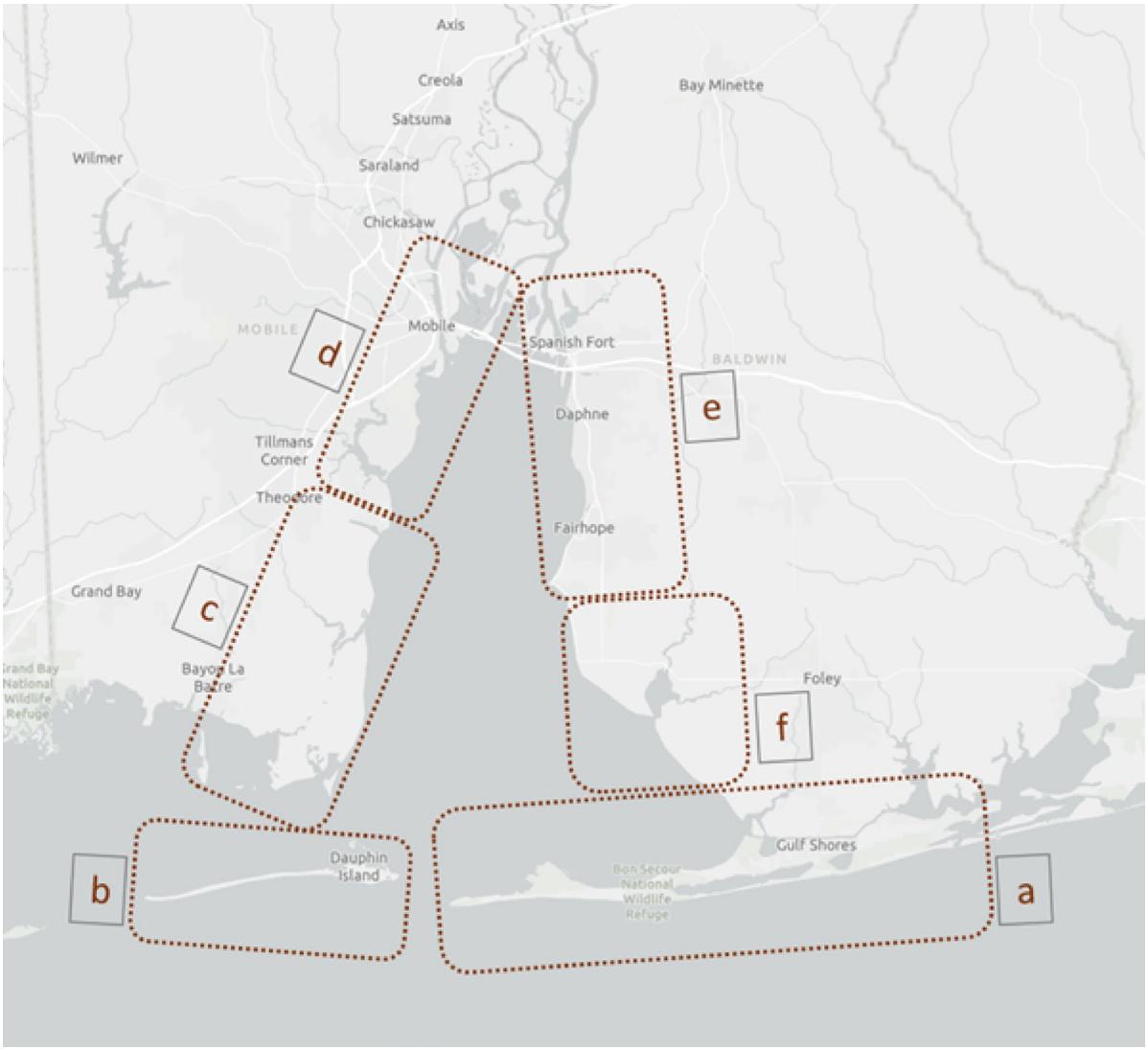



**Fig. 7** The Broken-Down ROIs Within the Study Area to Study Spatial Heterogeneity. The basemap was generated using ArcGIS Pro (version 3.7.0; Esri, https://www.esri.com/en-us/arcgis/products/arcgis-pro/overview), and the ROI boundaries and labels were added using Microsoft PowerPoint.

**Table 2** Descriptive statistics of the six ROIs mean yearly shoreline change rate.

| Site ID | Mean (m/yr) | Median | St. Dev | Min/Max | Interpretation |
|---|---|---|---|---|---|
| a | 0.33 | 0.39 | 1.83 | −2.95 / 7.13 | Highly variable accretion |
| b | −0.40 | −0.43 | 2.48 | −5.40 / 6.15 | Highly variable erosion |
| c | −0.05 | −0.007 | 1.20 | −4.64 / 3.26 | Low magnitude erosion, relatively stable |
| d | 0.75 | 0.89 | 1.03 | −0.82 / 4.90 | Mild accretion, relatively stable |
| e | 0.03 | 0.009 | 0.98 | −4.19 / 3.18 | Mild accretion, relatively stable |
| f | 0.38 | 0.34 | 0.52 | −0.57 / 1.79 | Mild accretion, relatively stable |

exhibit persistent accretion. Random erosion and accretion are also observed at localized transects across the study area.

The detailed analysis of Dauphin Island further shows a clear spatial contrast of persistence between its northern and southern (Fig. 9). The southern Gulf-facing shoreline is predominantly characterized by persistent erosion, indicating sustained long-term shoreline retreat rather than short-term episodic fluctuations. In contrast,

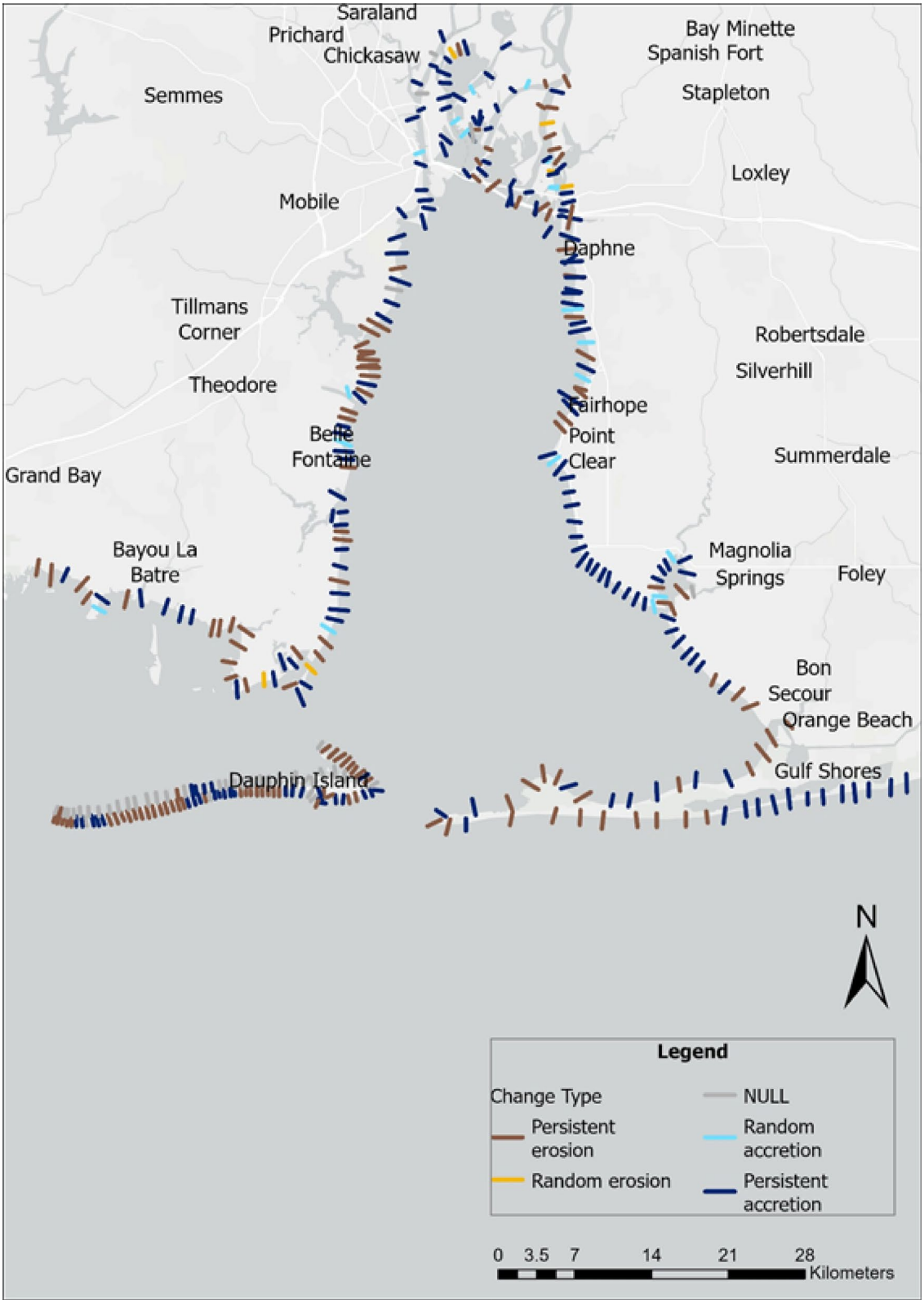



**Fig. 8** Map Showing Persistence or Randomness of Shoreline Change. Map generated using ArcGIS Pro (version 3.7.0; Esri, https://www.esri.com/en-us/arcgis/products/arcgis-pro/overview.

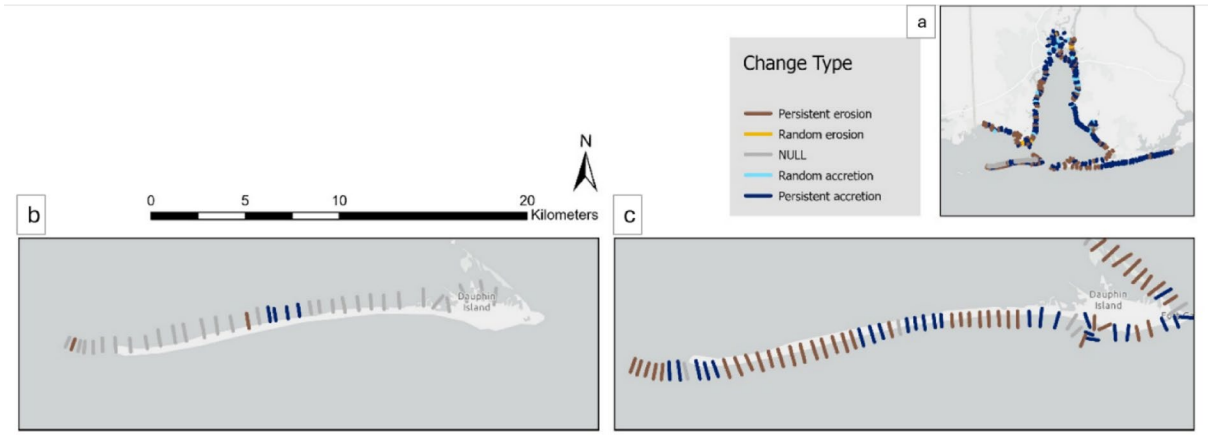



**Fig. 9** Spatial distribution of shoreline change persistence classifications in Mobile Bay. (**a**) Distribution of shoreline change classifications across the study area; (**b**) northern shoreline of Dauphin Island; and (**c**) southern, Gulf-facing shoreline of Dauphin Island.Map generated using ArcGIS Pro (version 3.7.0; Esri, https://www.esri.com/en-us/arcgis/products/arcgis-pro/overview.

most of the northern shoreline is stable, showing neither random erosion nor persistent erosion or accretion. A few portions of the northern shoreline exhibit persistent accretion and relatively limited erosion.

To assess how sensitive Hurst exponent estimates are to temporal interpolation, additional analyses were conducted for Dauphin Island (ROI b) using observed shoreline positions without interpolation in transects with observations in at least 20 distinct calendar years. Two approaches were evaluated: (1) annual aggregation of observed shoreline positions and (2) the longest uninterrupted sequence of observed monthly shoreline positions. Of the 106 transects, 60 met the temporal coverage criterion. Among these, 59 yielded valid paired Hurst exponent estimates in the annual sensitivity analysis, of which 56 (94.9%) retained their original persistent classification. The median difference between annual and original monthly Hurst estimates was -0.199. The monthly analysis yielded nine valid paired estimates, all of which retained their persistent classification, with a median difference of -0.217. These differences indicate that Hurst exponent estimates are sensitive to the temporal treatment of shoreline-position time series. Nevertheless, persistence classifications remained largely consistent across both sensitivity analyses. Because the supplementary approaches also differed from the original method in temporal resolution, observation length, and R/S estimation settings, the observed differences in Hurst exponent estimates cannot be attributed solely to interpolation.

## Temporal variability of shoreline change and hurricane impacts

To explore the temporal variability of shoreline behavior across Mobile Bay, monthly tidally corrected shoreline-change heatmaps are generated for each ROI.

The monthly heatmaps of shoreline displacement for the shore-normal transects shown in Fig. 10 capture shoreline dynamics on short time spans. Here, the available shoreline observations were aggregated to monthly time steps: a) using the mean when multiple observations occurred within a month; b) short gaps of up to two consecutive months were linearly interpolated, while longer gaps remained missing. The displacement was calculated relative to the first monthly shoreline position for each transect. Several ROIs exhibit frequent alternations between landward and seaward shoreline displacement over time, indicating continuous shoreline.

adjustment. ROI b, representing Dauphin Island, displays the highest short-term variability, with neighboring transects exhibiting repeated fluctuations in position. This response also resonates with the descriptive statistics shown in Table 2, which indicate that Dauphin Island has the most variable shoreline segment. ROIs d and e, located within the Mobile-Tensaw riverine estuarine system, exhibit similar changes but are more spatially

https://doi.org/10.1038/s41598-026-80664-1

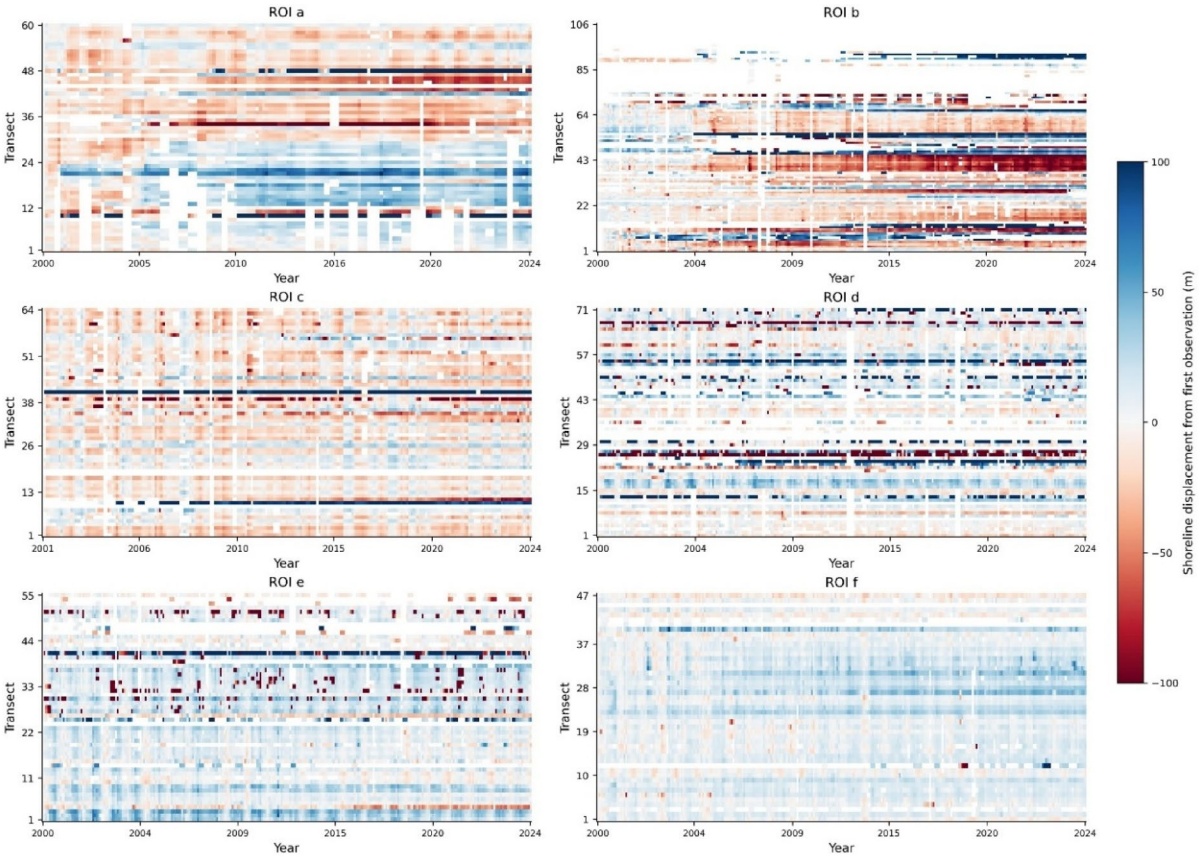



**Fig. 10** Monthly Heatmaps of tidally corrected shoreline displacement by ROI.

fragmented. ROI f exhibits comparatively stable shoreline conditions, while ROI c displays moderate variability with localized shoreline adjustments. To better identify broader long-term shoreline behavior and reduce short-term temporal variability, yearly shoreline heatmaps were subsequently analyzed in Fig. 11.

The yearly shoreline displacement heatmaps shown in Fig. 11 reveal how shoreline positions have changed relative to their initial location at each transect between 2000 and 2024. Here, available shoreline observations were aggregated by year using the mean when multiple observations occurred within a year. In this dataset, no annual interpolation was required. Shoreline displacement was calculated relative to the first yearly shoreline position for each transect. Bon Secour Bay, shown as ROI a, exhibits a clear spatial separation between the erosional (landward) and accretional (seaward) transects. The transects near the Florida panhandle generally exhibit seaward movement through time, while the transects near the Bon Secour Bay entrance exhibit more landward displacement after approximately 2007. The increasing intensity of red and blue in this figure indicates that shoreline change accumulated gradually rather than occurring as a single episodic event. ROI c shows more stable shoreline displacement. Most of the transects show lower displacement magnitudes, while several transects show gradual long-term displacement trends that become more prominent after 2010. These changes indicate cumulative longer-term shoreline adjustment rather than event-driven short-term fluctuations. ROI d and e both exhibit moderate spatial variability, with both erosional and accretional changes, but the displacement patterns are more fragmented and localized, unlike ROI b. ROI f is the most stable among all six ROIs. Dauphin Island, shown as ROI b, has the largest magnitude of shoreline displacement. Several transects show long-term ongoing shoreline erosion, with relative positions exceeding 50 to 100 m from the starting position, while very few transects show substantial seaward movement.

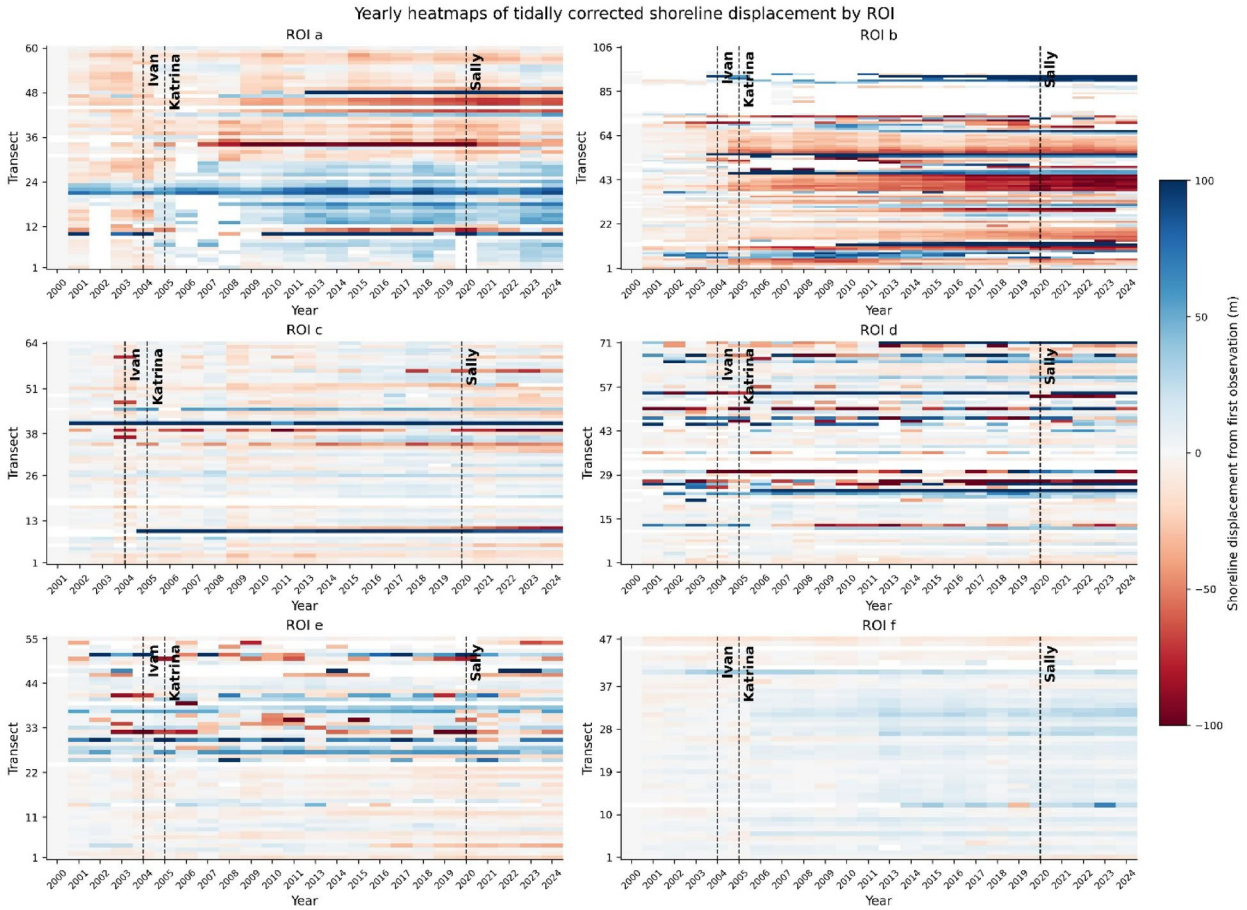



**Fig. 11** Yearly Heatmaps of tidally corrected shoreline displacement by ROI.

Shoreline displacement patterns associated with Hurricanes Ivan (2004), Katrina (2005), and Sally (2020) are shown in Fig. 12 and Fig. 13. To examine shoreline displacement associated with major hurricanes, annual mean shoreline positions were compared before and after Hurricanes, resulting in comparison periods of 2003–2005, 2004–2006, and 2019–2021, respectively. Transect-level displacement was calculated as the post-event minus pre-event annual mean shoreline position, with negative and positive values indicating landward and seaward displacement, respectively. The analysis was descriptive rather than inferential. Hurricanes Ivan (category 3) and Katrina (category 5) exhibited the largest shoreline displacements and the greatest variability among transects. At the same time, Hurricane Sally (category 2) produced smaller overall changes. Here, hurricane intensity referred to the Saffir-Simpson Hurricane Wind Scale, which classifies hurricanes according to maximum sustained wind speed as Category 1 (74–95 mph), Category 2 (96–110 mph), Category 3 (111 -129 mph), Category 4 (130–156 mph), and Category 5 (157 mph or higher), with Categories 3–5 classified as major hurricanes [53]. Most of the transects of the northern shore remained unchanged; only a few show accretions. More unstable transects are observed on the southern shore. The accreting transects on both the northern and southern shores are also the transects that show overall annual accretion, as shown in Fig. 5, in the opposite direction to the Mississippi sandbar.

The boxplot shown in Fig. 12 summarizes the overall distribution of shoreline displacement for each hurricane. Hurricane Ivan contains the largest individual displacement value; the median shoreline displacement for both Ivan and Katrina is negative, indicating that shoreline retreat was the dominant response across much of the island following these storms. Sally exhibits a smaller island-wide impact despite producing localized shoreline change. The presence of several large positive outliers for Ivan and Katrina also indicates that storm impacts include both

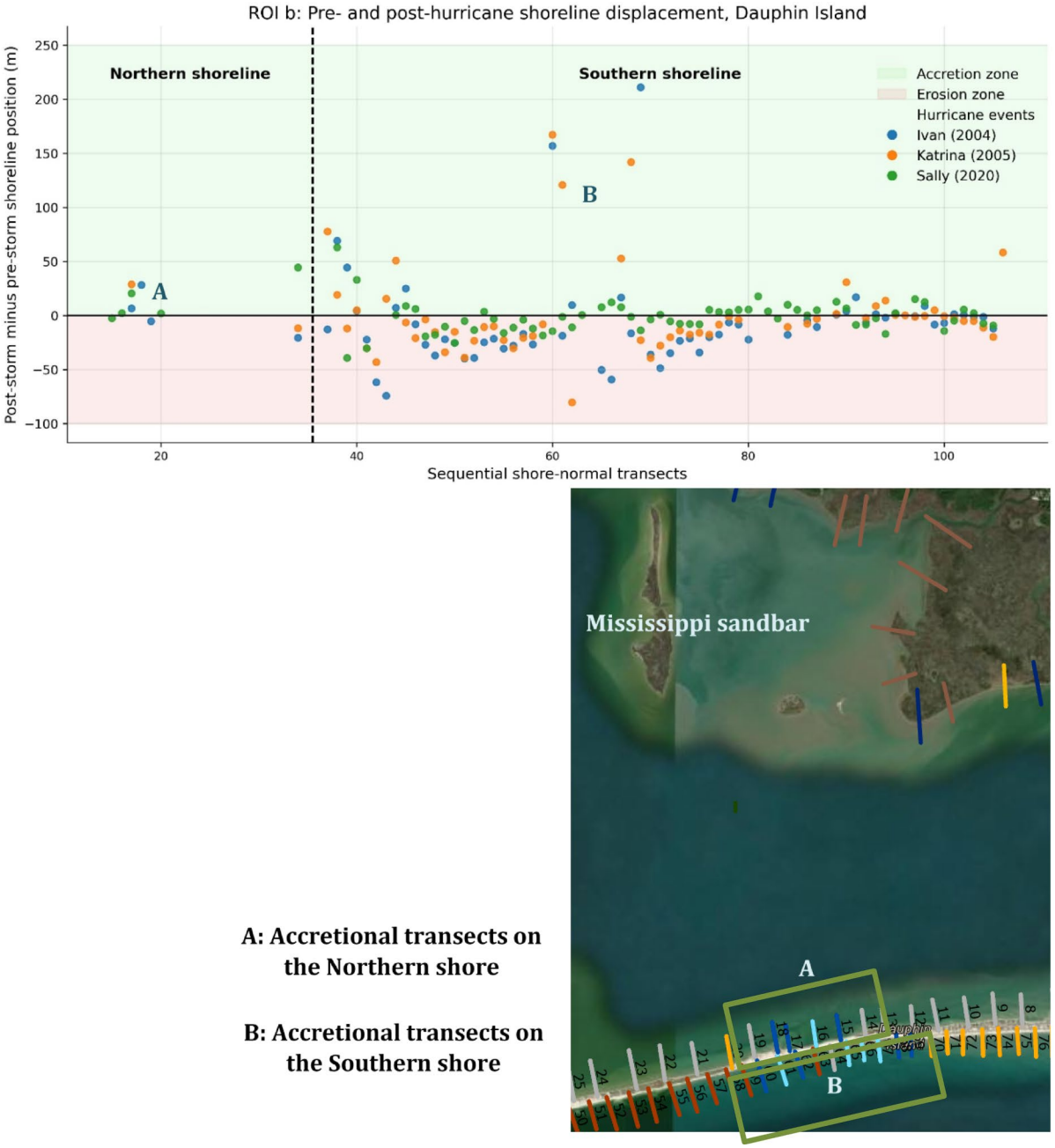



**Fig. 12** Shoreline displacement before and after hurricane events in Dauphin Island.

sediment deposition and erosion. Overall, both Figs. 11 and 12 suggest that storm impacts were characterized by substantial sediment redistribution along with some shoreline retreating across the island.

## Discussion

The results show that Mobile Bay's shoreline is spatially heterogeneous, with substantial differences in the magnitudes and directions of erosion and accretion, as well as in variability, across shore-normal transects. The discussion is organized into three parts. Building on previous studies, the first part discusses the spatiotemporal

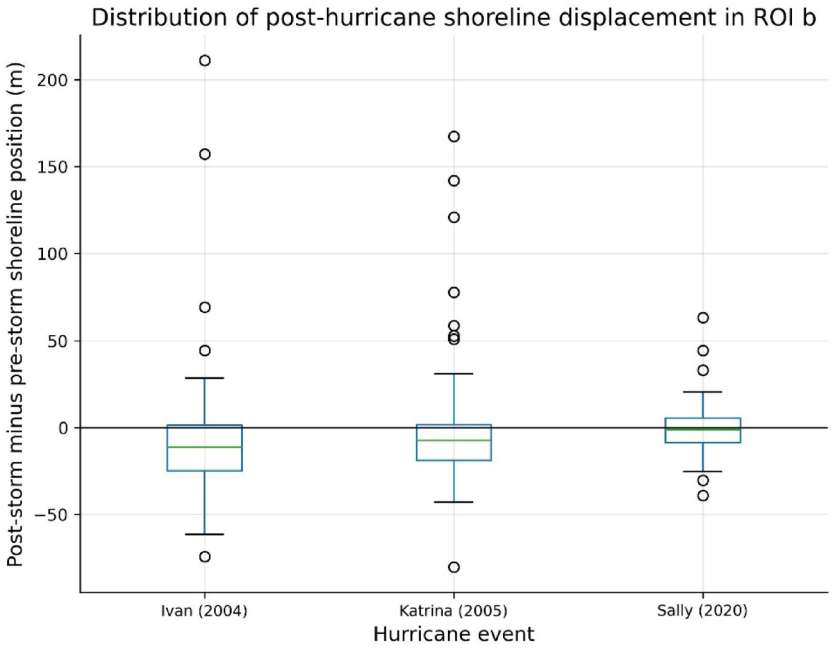



**Fig. 13** Distribution of Shreline displacement before and after hurricane events in Dauphin Island.

variability of shoreline change across Mobile Bay and provides geomorphological insight. Second part examines the implications of the observed shoreline behavior for Nature-Based Solutions and coastal management. The third part discusses the broader implications of the findings for coastal resilience and land management.

## Spatio-temporal variability of shoreline change

As shown in Figs. 4, 9 and 10, the riverine-estuarine environments represented by ROIs d and e exhibit a lower magnitude of shoreline displacement than the other ROIs, but greater localized variability (Table 2). These regions are influenced by freshwater discharge, sediment transport, and depositional processes associated with the Mobile-Tensaw River system, consistent with previous studies showing that the Mobile River Basin supplies substantial freshwater and sediment inputs that strongly influence estuarine hydrodynamics, salinity gradients, nutrient cycling, and sediment distribution throughout Mobile Bay[42,43]. The comparatively moderate and spatially fragmented shoreline changes observed in ROI d and e are consistent with the previously documented characteristics of the sheltered riverine-estuarine environment. In contrast, among all six ROIs, Dauphin Island (ROI b) exhibits the highest shoreline variability, the greatest erosion rates, and the strongest responses to major hurricane events. Furthermore, the northern and southern shores of Dauphin Island differ clearly. The heatmaps in Figs. 9 and 10 show that Dauphin Island has the most cumulative shoreline displacement and temporal variability during major hurricane periods. In contrast, the more sheltered estuarine shorelines generally experience smaller shoreline adjustments. These findings are consistent with prior literature identifying Dauphin Island as one of the most dynamic and vulnerable barrier island systems along the northern Gulf Coast[7,47,48]. Barrier islands are highly susceptible to overwash, dune breaching, storm surge, and longshore sediment transport during major hurricanes[54]. The southern shoreline facing the Gulf Coast experiences more shoreline displacement, whereas the northern shoreline experiences no substantial change. Previous studies have attributed differences between the northern and southern shorelines to wave exposure, longshore sediment transport, storm-surge impacts, and overwash processes associated with the Gulf-facing barrier island system[47,48]. Previous studies have also found that Dauphin Island is highly vulnerable to hurricane-induced shoreline retreat and sediment redistribution, particularly along its southern Gulf-facing shoreline, while the northern shoreline remains relatively sheltered due to reduced hydrodynamic energy within Mobile Bay[48,55]. The localized accretion seen in Dauphin

Island is consistent with previous studies, which describe the presence of the Mobile Pass ebb-tidal shoal system, including the Mississippi sand bar (Fig. 11), as a natural sediment bypass system that redistributes sand through east–west longshore transport[56,57]. The coexistence of adjacent erosional and accretional transects is consistent with the sediment-redistribution processes documented in these previous studies, while this study found more erosion than accretion. This also reflects the influence of coastal engineering interventions alongside natural coastal processes. During the study period, engineering interventions included post-hurricane sand placement, emergency berm construction, the Katrina Cut closure, and beach nourishment[49,58]. More recently, the 2024 East End Beach and Dune Restoration Project involved approximately 1.12 million cubic yards of sand placement, resulting in beaches approximately 400 feet wider, the creation of 60 acres of beach habitat and 20 acres of dune habitat, and the planting of approximately 693,000 native dune plants[59]. Therefore, EPR estimates for affected East End transects incorporate shoreline positions measured after engineered sand placement and should not be interpreted solely as indicators of natural shoreline evolution. Similarly, localized accretion and post-hurricane shoreline recovery cannot be attributed exclusively to natural sediment redistribution. Together, these patterns suggest that shoreline dynamics in Mobile Bay vary with coastal geomorphology and hydrodynamics. Similar spatial variability has been observed on neighboring northern Gulf Coast barrier islands in other studies[21,49]. A comparative analysis of Dauphin, Horn, and Petit Bois Islands found chronic erosion on the Gulf-facing side and deposition on the bay side of Dauphin Island, whereas the less-developed Mississippi barrier islands exhibited different shoreline-change patterns, highlighting the influence of local geomorphology, sediment transport, and human modification on barrier-island response[21]. Similarly, along the Florida Panhandle, 61% of the analyzed long-term shoreline-change transects were erosional, with an average erosional rate of approximately −0.9 m/yr[60]. These regional comparisons further demonstrate the spatial variability of shoreline response across northern Gulf Coast environments.

Along with wave exposure, tidal effects and sediment characteristics also influence sediment redistribution in the Mobile Bay area[61,62]. Previous studies characterize Mobile Bay as a shallow, microtidal estuary, where tidal and river-driven circulation interacts with spatially variable sediment environments, including the predominantly sandy barrier island environment of Dauphin Island and finer estuarine sediments[61]. Similar variability has been observed for beaches in estuaries and bays (BEBs), where shoreline response is strongly influenced by local wave conditions, tidal processes, and geomorphic setting. Rahbani et al.[63] identified spatial differences in wave energy among BEBs, while WinklerPrins et al.[64] found that ocean waves dominated near the bay entrance, whereas locally generated wind waves dominated farther inside the bay, with tidal conditions also causing variation in wave energy. Gallop et al.[65] further demonstrated that shifts in storm-wave direction can expose normally sheltered BEBs to increased wave energy and severe erosion. These previous studies demonstrate how interaction among wave conditions, tidal controls, and geomorphic setting can produce spatially variable shoreline responses within estuarine and bay environments[66], which is consistent with the spatial variability found in this study. Human modifications, particularly navigation-channel dredging and associated sediment management, can further alter sediment transport within the bay[33]. These interacting processes help explain why shoreline responses vary substantially between the exposed barrier-island and sheltered estuarine environments in this study.

The shoreline displacement observed following Hurricanes[26–28] further highlights the role of extreme events as a major driver of shoreline change on Dauphin Island. From 2000 to 2024, only two hurricanes made landfall on Mobile Bay. A Category 3 Hurricane Ivan on September 16, 2004, and a Category 2 Hurricane Sally on September 16, 2020[26,28]. Hurricane Katrina, which reached a Category 5 intensity in the Gulf of America in 2005, weakened to Category 3 and made landfall near the Louisiana-Mississippi border. Although Hurricane Katrina did not make direct landfall in Alabama, it still affected the Mobile Bay area, causing about 12 ft of storm surge and heavy damage around Mobile Bay and Dauphin Island[67],Sallenger et al., n.d.). The displacement analysis after the hurricane events in Fig. 11 shows that both Hurricanes Ivan and Katrina produced larger changes, mostly erosion and some accretion, among neighboring transects. This pattern suggests that storm impacts can be associated with sediment redistribution rather than uniform shoreline retreat. Similar storm-induced geomorphic reorganization has been documented along barrier islands throughout the Gulf Coast, where sediment is eroded

from some locations and deposited in others during and after major storm events[29,68], a pattern that should be accounted for in shoreline management planning.

### Implications for nature-based solutions (NBS) and coastal management

The observed spatial heterogeneity in shoreline behavior helps identify location-specific NBSs and other strategies for coastal management. Recent studies have emphasized that effective coastal adaptation strategies should be tailored to local geomorphic and hydrodynamic conditions[69,70]. As Dauphin Island is identified as highly dynamic and the most storm-sensitive within the study area, this suggests that adaptive sediment-based approaches, such as dune restoration, beach nourishment, and planting native dune vegetation, would be more effective than static shoreline stabilization measures. These approaches can help maintain sediment supply, accommodate natural shoreline adjustment, and enhance resilience to future storms. The 2024 East End Beach and Dune Restoration Project demonstrates the implementation of sediment-based restoration approaches on Dauphin Island, combining beach nourishment, dune habitat creation, and planting native dune vegetation[59]. Future coastal management strategies should therefore emphasize long-term monitoring of these interventions to evaluate shoreline stability, sediment retention, and resilience to subsequent storm events. The rest of Mobile Bay is a relatively sheltered estuarine environment, which makes it more suitable for living shorelines, marsh restoration, and oyster reef restoration. These NBS strategies reduce shoreline erosion, improve habitat quality, and provide ecosystem services while maintaining natural coastal processes[71,72]. Additionally, the comparatively stable conditions observed in ROIs c, d, e, and f indicate that these shoreline environments would be favorable for the long-term implementation of estuarine-based NBS strategies. Coordination among relevant agencies- Mobile Bay National Estuary Program, Alabama Department of Conservation and Natural Resources, USACE Mobile District, city and county offices and property owners, etc., is required to implement these NBSs.

### Broader implications for resilience and land management

In future climate scenarios, when sea-level rise and increased hurricane activity are in play, understanding both the magnitude and persistence of shoreline change becomes increasingly important for coastal resilience planning[73,74] to sustain such a densely populated area as Mobile Bay, which also supports critical habitats. The observed shoreline changes also have implications for coastal property management. In Alabama, gradual shoreline changes through accretion influence land gain in riparian property boundaries, whereas sudden shoreline changes caused by avulsive events, such as hurricanes, do not alter legal property boundaries[75]. The identified long-term erosion, accretion, and hurricane-induced shoreline displacement highlight the importance of understanding the spatial and temporal patterns of shoreline movement for coastal planning and land management. This study identified whether changes were due to avulsion (hurricane-induced displacement) or reliction (long-term erosion, as determined by persistence analysis). The identification of highly dynamic shoreline segments, particularly along Dauphin Island, provides valuable information for prioritizing adaptation efforts and directing resources toward areas most vulnerable to future coastal change. Overall, the findings demonstrate that integrating shoreline change rates with persistence analysis provides useful guidance to support site-specific coastal hazard management, land management, and resilience planning within Mobile Bay.

## Conclusion

Using the CoastSat toolkit, this study assessed shoreline change rates and investigates the persistence and randomness of shoreline change behavior in Mobile Bay. This study also integrated shoreline persistence analysis with conventional shoreline change-rate analysis to separate persistent erosion or accretion from episodic, or event-driven, variability.

The findings of this study reveal that shoreline change in Mobile Bay has been spatially and temporally heterogeneous in response to differences in the geomorphological characteristics of each site, indicating the need for site-specific coastal management strategies. Dauphin Island was a highly variable, erosional, high-energy coastal system with a mean change rate of −0.4 m/yr, a standard deviation of 2.48 m/yr, and individual transects ranging from −5.40 to 6.15 m/yr. The findings also demonstrate that the shoreline changes in Dauphin Island were associated with major hurricane events, highlighting the importance of considering both episodic and long-term shoreline processes in coastal management. So, here, adaptive NBS approaches are more appropriate than rigid restoration strategies. In contrast, Bon Secour Bay (ROI a) showed an overall accretional trend with a mean rate of 0.33 m/yr, while ROI d had the highest mean accretion rate of 0.75 m/yr. ROIs c and e showed comparatively low-magnitude changes, with mean rates of -0.05 and 0.03 m/yr, respectively. The comparatively stable and accretional conditions in these estuarine ROIs indicate greater suitability for long-term NBS approaches, such as marsh restoration and living shorelines.

While providing effective guidance for coastal risk management and adaptation strategies, this study has several limitations. First, the shoreline behavior was analyzed primarily from remotely sensed shoreline positions. It did not explicitly incorporate hydrodynamic processes, such as wave action, climate variability, sediment budgets, tidal currents, or nearshore engineering structures, all of which would affect shoreline evolution. Further process-based investigations can identify additional physical drivers that contribute to geomorphological dynamics in Mobile Bay. Second, the study area was relatively small and did not cover the entire Gulf Coast. Specific policy recommendations gained from this study are geographically bound. Third, the shoreline change rate was quantified using the End Point Rate (EPR) analysis method. This widely established, efficient, and simplified approach incorporates the earliest and latest shoreline positions and excludes intermediate observations, which is simpler than a regression-based approach. The present analysis also did not quantitatively separate shoreline changes associated with natural sediment redistribution from those associated with engineered sand placement and coastal restoration activities. Future studies could incorporate regression-based shoreline-change analyses alongside spatial and temporal records of engineering interventions to better characterize shoreline evolution and distinguish natural from engineered changes. Fourth, for validation, Google Earth reference imagery and corresponding Landsat imagery were not acquired on the same date but on nearby dates; the calculated positional differences could reflect short-term shoreline movement, differences in tidal and water-level conditions, and differences associated with shoreline delineation. Therefore, the MAE and RMSE values were interpreted as measures of image-to-image positional agreement rather than absolute CoastSat shoreline extraction error. Fifth, the persistence analysis using the Hurst exponent also had some limitations that stem from the irregular image availability. Shoreline observations were aggregated into month time steps, and images with shorter than two-month gaps were interpolated using linear interpolation; any longer gaps were excluded from the analysis. Hurst Analysis assumes regularly spaced observations, so the remaining temporal irregularities can bias the Hurst values. Thus, the Hurst results should be considered as an indicator of relative persistence rather than definitive long-term memory. Lastly, incorporating detailed topographic and bathymetric data or field observations for beach slope estimation, rather than using an SRTM-derived DEM to extract beach slope as a CoastSat parameter, would provide greater accuracy. The SRTM-derived DEM represented a static beach slope based on elevation data from 2000 and therefore did not account for potential changes in beach slope over the study period. This temporal limitation introduced uncertainty into the tidal correction, particularly in highly dynamic shoreline areas such as Dauphin Island. So, future studies should incorporate temporally varying beach slopes to improve the accuracy of tidal correction. Furthermore, although this study used the CoastSat toolkit to achieve sub-pixel shoreline detection, uncertainties remained associated with satellite image acquisition time, georeferencing accuracy, and shoreline delineation. Despite these limitations, the findings provide important insights into coastal land management, hazard preparedness, and resilience planning in this densely populated and ecologically significant region.

**Supplementary Information** The online version contains supplementary material available at https://doi.org/10.1038/s41598-026-80664-1.

**Author contributions** F.N. and W.S. conceived this study. F.N. contributed to collecting, processing, analyzing, and visualizing the data. F.N. wrote the first draft of the manuscript. H.D. and W.S. contributed to reviewing and editing the manuscript. D.N.M. contributed to reviewing the manuscript and providing comments. W.S. acquired the funding and supervised the study in its entirety.

**Funding** Funding for this project comes from the Department of the Treasury under Project 22-SFWS-248612-UAT, The Cooperative Institute for Research on Hydrology (CIROH) through the NOAA Cooperative Agreement with The University of Alabama (NA22NWS4320003).

**Data availability** Data associated with this study were deposited into the repository Figshare and are available at the following URL: https://figshare.com/articles/dataset/Supporting_Dataset_for_Spatiotemporal_Analysis_of_Shoreline_Change_in_Mobile_Bay/33107411. https://doi.org/10.6084/m9.figshare.33107411

## Declarations

**Competing interests** The authors declare no competing interests.

**Open Access** This article is licensed under a Creative Commons Attribution-NonCommercial-NoDerivatives 4.0 International License, which permits any non-commercial use, sharing, distribution and reproduction in any medium or format, as long as you give appropriate credit to the original author(s) and the source, provide a link to the Creative Commons licence, and indicate if you modified the licensed material. You do not have permission under this licence to share adapted material derived from this article or parts of it. The images or other third party material in this article are included in the article's Creative Commons licence, unless indicated otherwise in a credit line to the material. If material is not included in the article's Creative Commons licence and your intended use is not permitted by statutory regulation or exceeds the permitted use, you will need to obtain permission directly from the copyright holder. To view a copy of this licence, visit http://creativecommons.org/licenses/by-nc-nd/4.0/.

## References

1. Misra, A. & Balaji, R. A study on the shoreline changes and land-use/ land-cover along the South Gujarat coastline. *Procedia Eng.***116**, 381–389. https://doi.org/10.1016/j.proeng.2015.08.311 (2015).
2. Pang, T., Wang, X., Nawaz, R. A., Keefe, G. & Adekanmbi, T. Coastal erosion and climate change: A review on coastal-change process and modeling. *Ambio***52**(12), 2034–2052. https://doi.org/10.1007/s13280-023-01901-9 (2023).
3. Talke, S. A. & Jay, D. A. Changing tides: The role of natural and anthropogenic factors. *Annu. Rev. Mar. Sci.***12**, 121–151. https://doi.org/10.1146/annurev-marine-010419-010727 (2020).
4. Vitousek, S. et al. Scalable, data-assimilated models predict large-scale shoreline response to waves and sea-level rise. *Sci. Rep.***14**(1), 28029 (2024).
5. Luijendijk, A. et al. The state of the world's beaches. *Sci. Rep.***8**(1), 6641. https://doi.org/10.1038/s41598-018-24630-6 (2018).
6. Mentaschi, L., Vousdoukas, M. I., Pekel, J.-F., Voukouvalas, E. & Feyen, L. Global long-term observations of coastal erosion and accretion. *Sci. Rep.***8**(1), 12876. https://doi.org/10.1038/s41598-018-30904-w (2018).
7. Boak, E. H. & Turner, I. L. Shoreline definition and detection: A review. *J. Coastal Res.***21**(4), 688–703. https://doi.org/10.2112/03-0071.1 (2005).
8. Vitousek, S. et al. Doubling of coastal flooding frequency within decades due to sea-level rise. *Sci. Rep.***7**(1), 1399. https://doi.org/10.1038/s41598-017-01362-7 (2017).
9. Thieler, E. R., Himmelstoss, E. A., Zichichi, J. L., & Ergul, A. *The Digital Shoreline Analysis System (DSAS) version 4.0-an ArcGIS extension for calculating shoreline change* [U.S. Geological Survey Open-File Report 2008–1278.]. US Geological Survey. https://cmgds.marine.usgs.gov/publications/DSAS/of2008-1278/ (2009).
10. Smith, K. E. L., Terrano, J. F., Pitchford, J. L. & Archer, M. J. Coastal wetland shoreline change monitoring: A comparison of shorelines from high-resolution WorldView satellite imagery, aerial imagery, and field surveys. *Remote Sens.*https://doi.org/10.3390/rs13153030 (2021).
11. Vos, K. et al. Benchmarking satellite-derived shoreline mapping algorithms. *Commun. Earth Environ.***4**(1), 345. https://doi.org/10.1038/s43247-023-01001-2 (2023).
12. Seale, C., Redfern, T., Chatfield, P., Luo, C. & Dempsey, K. Coastline detection in satellite imagery: A deep learning approach on new benchmark data. *Remote Sens. Environ.***278**, 113044. https://doi.org/10.1016/j.rse.2022.113044 (2022).

13. Ankrah, J., Monteiro, A., & Madureira, H. Bibliometric analysis of data sources and tools for shoreline change analysis and detection. *Sustainability*, *14*(9). https://doi.org/10.3390/su14094895 (2022).
14. Tsiakos, C.-A.D. & Chalkias, C. Use of machine learning and remote sensing techniques for shoreline monitoring: A review of recent literature. *Appl. Sci.*https://doi.org/10.3390/app13053268 (2023).
15. Hapke, C. J., Kratzmann, M. G. & Himmelstoss, E. A. Geomorphic and human influence on large-scale coastal change. *Geomorphology***199**, 160–170. https://doi.org/10.1016/j.geomorph.2012.11.025 (2013).
16. Vos, K., Splinter, K. D., Harley, M. D., Simmons, J. A. & Turner, I. L. CoastSat: A Google Earth Engine-enabled Python toolkit to extract shorelines from publicly available satellite imagery. *Environ. Model. Softw.***122**, 104528. https://doi.org/10.1016/j.envsoft.2019.104528 (2019).
17. Souiri, S., Hakkou, M., Haddaoui, H., Oubdil, S., & Lmrimed, N. Automatic Coastline Detection Using CoastSat Toolbox and GIS: A Case Study at Oued-Laou Beach, Morocco. *E3S Web of Conferences*, *607*, 04024. https://doi.org/10.1051/e3sconf/202560704024 (2025).
18. López, L., Cellone, F., Guardo, N. & Carol, E. Semi-automated shoreline extraction applied to estuarine coasts: A case study in the Río de la Plata estuary, Argentina. *Estuar. Coast. Shelf Sci.***314**, 109142. https://doi.org/10.1016/j.ecss.2025.109142 (2025).
19. Gunasinghe, G. P. et al. Monsoon-driven geomorphological changes along the west coast of Sri Lanka: A combined approach utilizing 'CoastSat' and Google Earth Engine. *Ocean Sci. J.***57**(3), 475–492. https://doi.org/10.1007/s12601-022-00081-z (2022).
20. Curoy, J., Ward, R. D., Barlow, J., Moses, C. & Nakhapakorn, K. Coastal dynamism in Southern Thailand: An application of the CoastSat toolkit. *PLoS ONE***17**(8), e0272977. https://doi.org/10.1371/journal.pone.0272977 (2022).
21. Asare-Bediako, B. et al. Shoreline change detection along the eastern coast of Ghana: Leveraging GIS and advanced remote sensing techniques. *Sci. Rep.***15**(1), 33032. https://doi.org/10.1038/s41598-025-98260-0 (2025).
22. Alarcon, V. J. & McAnally, W. H. A strategy for estimating nutrient concentrations using remote sensing datasets and hydrological modeling. *Int. J. Agric. Environ. Inform. Syst. (IJAEIS)***3**(1), 1–13. https://doi.org/10.4018/jaeis.2012010101 (2012).
23. NOAA National Marine Fisheries Service. *Habitation Connections: Wetlands, Fisheries and Economics, Part Four: Wetlands, Fisheries, and Economics in the Gulf of Mexico.* U.S. Department of Commerce. http://www.nmfs.noaa.gov/habitat/habitatconservation/publications/habitatconections/num4.htm. (2009).
24. Dey, H., Shao, W., Pan, S. & Tian, H. The spatiotemporal patterns of community vulnerability in the U.S. Mobile Bay from 2000–2020. *Appl. Spat. Anal. Policy***17**(1), 371–392. https://doi.org/10.1007/s12061-023-09549-4 (2024).
25. Scott, J. C., & Bohman, L. R. Hurricane Frederic tidal floods of September 12–13, 1979, along the Gulf Coast, Pine Beach, St. Andrews Bay, and Fort Morgan quadrangles, Alabama. In *Hydrologic Atlas* (No. 634). U.S. Geological Survey. https://doi.org/10.3133/ha634 (1980).
26. Berg, R., & Reinhart, B. National hurricane center tropical cyclone report: Hurricane Sally (AL 192020). *National Oceanic and Atmospheric Administration, National Weather Service, Washington, DC*. https://www.nhc.noaa.gov/data/tcr/AL192020_Sally.pdf (2021).
27. Sallenger, A., Wright, C. W., & Lillycrop, J. (n.d.). Coastal-Change Impacts during Hurricane Katrina: An Overview. In *Coastal Sediments '07* (pp. 888–896). https://doi.org/10.1061/40926(239)68
28. Stewart, S. R. Tropical cyclone report—Hurricane Ivan 2–24 September 2004. *National Hurricane Center*, *40*. http://www.nhc.noaa.gov/2004ivan.shtml (2005).
29. Morton, R. A. *National Assessment of Shoreline Change: Part 1: Historical Shoreline Changes and Associated Coastal Land Loss Along the US Gulf of Mexico* (Diane Publishing, 2008).
30. Cass, E., Shao, W., Hao, F. & Moradkhani, H. An online survey analysis of coastal flood recovery aided by resident mitigation behavior. *Nat. Hazards***121**(12), 14355–14371. https://doi.org/10.1007/s11069-025-07357-2 (2025).
31. Lewis, M., Moftakhari, H. & Passalacqua, P. Challenges for compound coastal flood risk management in a warming climate: A case study of the Gulf Coast of the United States. *Front. Water*https://doi.org/10.3389/frwa.2024.1405603 (2024).
32. Santiago-Collazo, F. L., Bilskie, M. V. & Hagen, S. C. A comprehensive review of compound inundation models in low-gradient coastal watersheds. *Environ. Model. Softw.***119**, 166–181. https://doi.org/10.1016/j.envsoft.2019.06.002 (2019).
33. Passeri, D., Long, J. W., Jenkins III, R. L., & Thompson, D. *Effects of proposed navigation channel improvements on sediment transport in Mobile Harbor, Alabama* (Report Nos. 2018–1123; Open-File Report). USGS Publications Warehouse. https://doi.org/10.3133/ofr20181123 (2018).
34. National Oceanic and Atmospheric Administration. (n.d.). *Continually Updated Shoreline Product (CUSP)*. NOAA Shoreline. https://shoreline.noaa.gov/cusp.html
35. Masson-Delmotte, V. et al. Climate change 2021: The physical science basis. *Contribut. Working Group I to the Sixth Assessment Rep. Intergovern. Panel on Climate Change***2**(1), 2391. https://doi.org/10.1017/9781009157896.001 (2021).
36. Organization, W. M. WMO guidelines on the calculation of climate normals. *World Meteorological Organization. Geneva*. https://community.wmo.int/en/wmo-climatological-normals (2017).

37. Gómez-Pazo, A., Payo, A., Paz-Delgado, M. V. & Delgadillo-Calzadilla, M. A. Open digital shoreline analysis system: ODSAS v1.0. *J. Marine Sci. Eng.*https://doi.org/10.3390/jmse10010026 (2022).
38. Estes, M. G. Jr. et al. A modeling system to assess land cover land use change effects on SAV habitat in the Mobile Bay Estuary. *JAWRA J. Am. Water Resour. Assoc.***51**(2), 513–536. https://doi.org/10.1111/jawr.12263 (2015).
39. U.S. Census Bureau. *2020 Census Gazetteer Files*. United States Census Bureau. https://www.census.gov/geographies/reference-files/2020/geo/gazetter-file.html (2020).
40. Danielson, J. J., Brock, J. C., Howard, D. M., Gesch, D. B., Bonisteel-Cormier, J. M., & Travers, L. J. Topobathymetric model of Mobile Bay, Alabama. *US Geol. Surv. Data Series*, *769*(6). (2013).
41. Handley, L., Spear, K., Jones, S., & Thatcher, C. *Mobile Bay* (Report K). USGS Publications Warehouse. https://pubs.usgs.gov/publication/70041785 (2013).
42. Lehrter, J. C. Regulation of eutrophication susceptibility in oligohaline regions of a northern Gulf of Mexico estuary, Mobile Bay, Alabama. *Mar. Pollut. Bull.***56**(8), 1446–1460 (2008).
43. Pennock, J. R., Boyer, J. N., Herrera-Silveira, J. A., Iverson, R. L., Whitledge, T., Mortazavi, B., & Comin, F. A. Nutrient behavior and phytoplankton production in Gulf of Mexico estuaries. *Biogeochem. Gulf of Mexico Estuaries*, 109–162. (1999).
44. Danielson, J. J., Poppenga, S. K., Brock, J. C., Evans, G. A., Tyler, D. J., Gesch, D. B., Thatcher, C. A., & Barras, J. A. *Topobathymetric Model of Mobile Bay, Alabama* (U.S. Geological Survey Data Series No. 769). U.S. Geological Survey. https://doi.org/10.3133/ds769 (2013).
45. Dykstra, S. L. & Dzwonkowski, B. The propagation of fluvial flood waves through a backwater-estuarine environment. *Water Resour. Res.***56**(2), e2019WR025743. https://doi.org/10.1029/2019WR025743 (2020).
46. Douglas, B. C. & Mark Crowell. Long-term shoreline position prediction and error propagation. *J. Coastal Res.*, *16*(1), 145–152. JSTOR. http://www.jstor.org/stable/4300019 (2000).
47. Morton, R. A., Miller, T. & Moore, L. Historical shoreline changes along the US Gulf of Mexico: A summary of recent shoreline comparisons and analyses. *J. Coast. Res.***21**(4), 704–709. https://doi.org/10.2112/04-0230.1 (2005).
48. Douglass, S. L. Beach Erosion and Deposition on Dauphin Island, Alabama, U.S.A. *J. Coastal Res.*, *10*(2), 306–328. JSTOR. http://www.jstor.org/stable/4298218 (1994).
49. Smith, C., Long, J. W., Henderson, R. E., & Nelson, P. *Assessing the impact of open-ocean and back-barrier shoreline change on Dauphin Island, Alabama, at multiple time scales over the last 75 years* (Report Nos. 2018–1170; Open-File Report). USGS Publications Warehouse. https://doi.org/10.3133/ofr20181170 (2018).
50. Byrnes, M. R., & Berlinghoff, J. L. *Sediment Dynamics in Mobile Bay, Alabama: Development of an Operational Sediment Budget* [Mobile Bay National Estuary Program]. Applied Coastal Research and Engineering, Inc. http://www.mobilebaynep.com/images/uploads/library/mobile_bay_sediment_budget_final_report_plus_appendices_032013.pdf (2013).
51. Xu, H. Modification of normalised difference water index (NDWI) to enhance open water features in remotely sensed imagery. *Int. J. Remote Sens.***27**(14), 3025–3033. https://doi.org/10.1080/01431160600589179 (2006).
52. Liu, Q., Trinder, J. C. & Turner, I. L. Automatic super-resolution shoreline change monitoring using Landsat archival data: A case study at Narrabeen–Collaroy Beach, Australia. *J. Appl. Remote Sens.*https://doi.org/10.1117/1.JRS.11.016036 (2017).
53. National Hurricane Center. (n.d.). *Saffir-Simpson Hurricane Wind Scale*. National Oceanic and Atmospheric Administration. National Hurricane Center and Central Pacific Hurricane Center. Retrieved September 23, from https://www.nhc.noaa.gov/aboutsshws.php (2026).
54. Stockdon, H. F., Sallenger, A. H., Holman, R. A. & Howd, P. A. A simple model for the spatially-variable coastal response to hurricanes. *Mar. Geol.***238**(1), 1–20. https://doi.org/10.1016/j.margeo.2006.11.004 (2007).
55. Park, K., Powers, S. P., Bosarge, G. S. & Jung, H.-S. Plugging the leak: Barrier island restoration following Hurricane Katrina enhances larval retention and improves salinity regime for oysters in Mobile Bay, Alabama. *Mar. Environ. Res.***94**, 48–55. https://doi.org/10.1016/j.marenvres.2013.12.003 (2014).
56. Byrnes, M. R., Rosati, J. D., Griffee, S. F. & Berlinghoff, J. L. Historical sediment transport pathways and quantities for determining an operational sediment budget: Mississippi Sound Barrier Islands. *J. Coast. Res.***63**(sp1), 166–183. https://doi.org/10.2112/SI63-014.1 (2013).
57. Rosati, J. D. et al. Coastal inlet navigation research in the US Army Corps of Engineers. *Coastal Dyn.***7**, 15–24 (2013).
58. Froede, C. R. Jr. Elevated waves erode the western end of the recently completed sand berm on Dauphin Island, Alabama (U.S.A). *J. Coast. Res.***236**, 1602–1604. https://doi.org/10.2112/07A-0019.1 (2007).
59. Town of Dauphin Island. *East End Beach and Dune Restoration*. Town of Dauphin Island. https://www.townofdauphinisland.org/di-east-end-beach-dune-restoration (2024).
60. Kratzmann, M. *U.S. Geological Survey national shoreline change—Summary statistics for updated vector shorelines (1800s–2010s) and associated shoreline change data for the Georgia and Florida coasts* (Report No. 1156; Data Report, p. 8). USGS Publications Warehouse. https://doi.org/10.3133/dr1156 (2022).

61. Jenkins III, R. L., Long, J. W., Dalyander, P. S., Thompson, D. M., & Mickey, R. C. *Development of a process-based littoral sediment transport model for Dauphin Island, Alabama* (U.S. Geological Survey Open-File Report 2008–1278. Nos. 2020–1011; p. 43). U.S. Geological Survey. https://doi.org/10.3133/ofr20201011 (2020).
62. Ralston, D. K. et al. Interacting influences of diurnal tides, winds, and river discharge on a large coastal plume. *J. Geophys. Res. Oceans***129**(9), e2024JC021288. https://doi.org/10.1029/2024JC021288 (2024).
63. Rahbani, M. et al. Spatial patterns in wave signatures on beaches in estuaries and bays. *Geomorphology***398**, 108070. https://doi.org/10.1016/j.geomorph.2021.108070 (2022).
64. WinklerPrins, L. et al. Components and Tidal Modulation of the Wave Field in a Semi-enclosed Shallow Bay. *Estuaries Coasts***46**(3), 645–659. https://doi.org/10.1007/s12237-022-01154-x (2023).
65. Gallop, S. L. et al. Wave direction shift triggered severe erosion of beaches in estuaries and bays with limited post-storm recovery. *Earth Surf. Process. Landf.***45**(15), 3854–3868. https://doi.org/10.1002/esp.5005 (2020).
66. Vila-Concejo, A. et al. Morphodynamics and management challenges for beaches in modified estuaries and bays. *Cambridge Prisms: Coastal Futures***2**, e11. https://doi.org/10.1017/cft.2024.7 (2024).
67. Abdelhafez, M. A., Ellingwood, B. & Mahmoud, H. Vulnerability of seaports to hurricanes and sea level rise in a changing climate: A case study for Mobile, AL. *Coast. Eng.***167**, 103884. https://doi.org/10.1016/j.coastaleng.2021.103884 (2021).
68. Otvos, E. G. & Carter, G. A. Regressive and transgressive barrier islands on the North-Central Gulf Coast—Contrasts in evolution, sediment delivery, and island vulnerability. *Geomorphology***198**, 1–19. https://doi.org/10.1016/j.geomorph.2013.05.015 (2013).
69. Sutton-Grier, A. E., Wowk, K. & Bamford, H. Future of our coasts: The potential for natural and hybrid infrastructure to enhance the resilience of our coastal communities, economies and ecosystems. *Environ. Sci. Policy***51**, 137–148. https://doi.org/10.1016/j.envsci.2015.04.006 (2015).
70. Temmerman, S. et al. Ecosystem-based coastal defence in the face of global change. *Nature***504**(7478), 79–83. https://doi.org/10.1038/nature12859 (2013).
71. Morris, R. L., Konlechner, T. M., Ghisalberti, M. & Swearer, S. E. From grey to green: Efficacy of eco-engineering solutions for nature-based coastal defence. *Glob. Change Biol.***24**(5), 1827–1842. https://doi.org/10.1111/gcb.14063 (2018).
72. Narayan, S. et al. The effectiveness, costs and coastal protection benefits of natural and nature-based defences. *PLoS ONE***11**(5), 1–17. https://doi.org/10.1371/journal.pone.0154735 (2016).
73. Legg, S. *Interaction*, *49*(4), 44–45. https://doi.org/10.3316/informit.315096509383738 (2021).
74. Sweet, W. V., Hamlington, B. D., Kopp, R. E., Weaver, C. P., Barnard, P. L., Bekaert, D., Brooks, W., Craghan, M., Dusek, G., Frederikse, T., & others. *Global and regional sea level rise scenarios for the United States*. https://doi.org/10.7289/v5/tr-nos-coops-083 (2022).
75. Duggan, J. D., Bearden, B. L., & Guthrie, G. M. When the Dam Breaks—The Avulsion That Sparked a Property Dispute. *The Wave*, *47*(2), 13–15. https://www.kelmanonline.com/httpdocs/files/AWEA/thewave-summer2026/index.html (2026).

**Publisher's note** Springer Nature remains neutral with regard to jurisdictional claims in published maps and institutional affiliations.

## Authors and Affiliations

**Fatema Tuz Johra Nourin[1] · Hemal Dey[1,3] · Wanyun Shao[1,2,3] · Dinuke Munasinghe[1,3]**

✉ Wanyun Shao
wshao1@ua.edu

[1] Department of Geography and the Environment, University of Alabama, Tuscaloosa, USA

[2] Institute for Social Science Research, University of Alabama, Tuscaloosa, USA

[3] Alabama Water Institute, University of Alabama, Tuscaloosa, USA